HSE

Health and Safety Executive

Flammable vapour cloud risks from tank overfilling incidents

Prepared by the **Health and Safety Laboratory**
for the Health and Safety Executive 2012

RR937
Research Report

HSE

Health and Safety Executive

Flammable vapour cloud risks from tank overfilling incidents

GT Atkinson & SE Gant
Health and Safety Laboratory
Harpur Hill
Buxton
Derbyshire
SK17 9JN

This report documents research undertaken in 2007 and 2008 to examine the important factors affecting the production of flammable vapour in incidents where large storage tanks of volatile liquids are overfilled. This is an important output from the Buncefield response programme that was not published on completion due to constraints on HSL staff involved in the investigation arising from the legal case. The work was summarised for the Process Safety Leadership report but has not been published in full.

It includes much useful information arising from a joint study of tank designs carried out with Shell Global Solutions. The analysis describes how different tank designs are likely to behave in an overflow situation, and the impact on the production rate of flammable vapour. It also contains the results of some early Computational Fluid Dynamics (CFD) modelling studies into the vapourisation of volatile components of multi component hydrocarbon mixtures. Simulations are presented that examine the effect of a number of factors on the vapour cloud behaviour, including the bund shape and location, tank proximity, presence of obstacles and spray pattern from the overfilling tank.

The work provides a first step towards developing a mathematical model to predict the size of flammable vapour clouds from overfilling releases, based on simple measures such as the tank dimensions, tank design type, pumping rates and liquid composition.

This work highlights the fact that there are important processes occurring at the bottom of the cascade near to the tank base that were not well understood at the time the report was completed, most notably splashing and pool evaporation. These issues have been explored in a later research report RR908.

This report and the work it describes were funded by the Health and Safety Executive (HSE). Its contents, including any opinions and/or conclusions expressed, are those of the authors alone and do not necessarily reflect HSE policy.

HSE Books

© Crown copyright 2012

First published 2012

You may reuse this information (not including logos) free of charge in any format or medium, under the terms of the Open Government Licence. To view the licence visit www.nationalarchives.gov.uk/doc/open-government-licence/, write to the Information Policy Team, The National Archives, Kew, London TW9 4DU, or email psi@nationalarchives.gsi.gov.uk.

Some images and illustrations may not be owned by the Crown so cannot be reproduced without permission of the copyright owner. Enquiries should be sent to copyright@hse.gsi.gov.uk.

ACKNOWLEDGEMENTS

The authors would like to thank Les Shirvill and Aziz Ungut from Shell Global Solutions (UK) and Peter Kerkhof (Shell Global Solutions International and Deputy Chairman of EEMUA) for help in providing information on tank designs and incidents.

CONTENTS

EXECUTIVE SUMMARY

This report documents ongoing research aimed at understanding the important factors affecting the production of flammable vapour in incidents where large storage tanks of volatile liquids are overfilled. The work provides a first step towards developing a mathematical model which will predict the likely size of flammable vapour clouds based on simple measures such as the tank dimensions, tank design type, pumping rates and liquid composition.

Three main types of storage tank are identified which are each likely to produce different flow behaviour in the event of overfilling: fixed roof tanks with vents, fixed roof tanks with pressure/vacuum valves and floating deck tanks with no fixed roof. The likely release scenarios from overfilling each of the tank designs are discussed.

Computational Fluid Dynamics (CFD) simulations show that the rate at which liquid is vaporised in tank-overfilling incidents is mainly affected by the size of the spray droplets, the distribution of the spray around the circumference of the tank and the width of the spray. A fine spray of droplets over a large area will lead to the highest vapour production rates.

The size of the flammable cloud appears to be not solely a function of the vaporisation rate. CFD simulations show that the design and location of the bund wall and the presence of obstacles around the tank also affect the size of the flammable cloud due to their influence on dispersion of the vapour. This suggests that a model for predicting the size of flammable vapour clouds needs to take account of the location of the tank and its surroundings as well as the tank dimensions, pumping rate, liquid composition etc. To minimise complexity, one option would be to base a model on a 'worst case' scenario. Preliminary CFD analysis presented here indicates that a vertical bund wall next to the tank would produce the largest flammable cloud. The distance from the bund wall to the tank is shown to affect the size of the cloud and this requires further study to identify the worst case situation.

It is recommended that detailed experiments be undertaken to help quantify the likely size distribution of droplets produced by tank overfilling releases. The breakup of liquid flowing from a tank into filaments and droplets cannot be predicted reliably at present. It is important to determine the likely size of droplets as this strongly affects the amount of vapour produced and the flammable cloud size.

In a tank overfilling incident a pool of liquid forms in the bunded area around the tank. All of the CFD simulations undertaken in this work ignore any vapour produced from the surface of this pool. Initial tests using the pool-evaporation model, GASP, and consideration of the likely mass transfer rates show that this matter should be investigated further. Two alternative approaches to simulate pool evaporation using CFD models are outlined. To provide confidence in the accuracy of these techniques, it is recommended that a short validation study be undertaken, comparing the two models' performance against GASP and experimental data in a simple pool evaporation scenario. Once the accuracy of the models has been proven, the tank overfilling case should be examined.

The CFD simulations presented here also model the droplets as "disappearing" on contact with the floor of the bund whereas in reality there is likely to be significant splashing as the droplets impinge onto the wetted bund floor and rebound. Splashing is likely to have two effects: a reduction in the speed of the vapour flowing across the bund and an increase in the vapour concentration. Future modelling of tank overfilling releases should examine the significance of these effects.

1 INTRODUCTION

On the morning of 11th December 2005 there was a large explosion and fire at the Buncefield Oil Storage Depot, near Hemel Hempstead. The subsequent investigation into the incident indicated that the explosion had been caused by ignition of a large flammable vapour cloud that was produced by overfilling of one of the large petrol tanks on the site [1-3]. Records indicated that approximately 200 tonnes of petrol was released from one of the tanks over a 23-minute period. When the tank was overfilled, petrol flowed from vents on the roof of the tank and cascaded over the tank sides, falling around 15 metres to the floor. As the liquid fuel fell through the air, it partially evaporated and produced a dense, vapour-rich cloud. This dense cloud then spread over a considerable area across the Buncefield site before it was ignited. There have previously been other major incidents involving ignition of a vapour cloud produced by sprays of volatile liquids from tank overfilling, e.g. Naples harbour fuel storage depot, Italy in 1985 [4] and Sri Racha Refinery, Thailand in 1999 [5].

In the wake of the Buncefield Incident, there is a need to reassess the risks posed by other fuel depots around the UK. The purpose of the current report is to document ongoing research aimed at predicting the amount of flammable vapour generated by tank overfilling releases. It is difficult to undertake experiments on a scale similar to the Buncefield incident due to safety and environmental constraints. Instead, much of the analysis presented in this report is based on mathematical models.

The report comprises four main sections. The following section describes the types of tanks commonly used in the UK for storage of crude oil and other volatile hydrocarbon products. The likely release scenarios from overfilling releases for each of the tank designs is discussed in the subsequent section. Section 4 presents results from modelling various release scenarios using CFD. Finally, Section 5 provides some conclusions and recommendations for further work.

2 TANK INSTALLATIONS

There are three main classes of tanks used to store liquid hydrocarbons in the UK:

- Fixed roof tanks with vents (FRV)
- Fixed roof tanks with pressure/vacuum valves (FRPVV)
- Floating deck tanks with no fixed roof (FD)

There are other types of tanks, for example fixed-roof tanks with internal floating decks. However, for the purposes of this study, we are interested primarily in how a spray is formed from an overfilling incident and the internal structure of the tank is not important. Examples of the three types of tank are shown in Figure 1, 2 and 3.

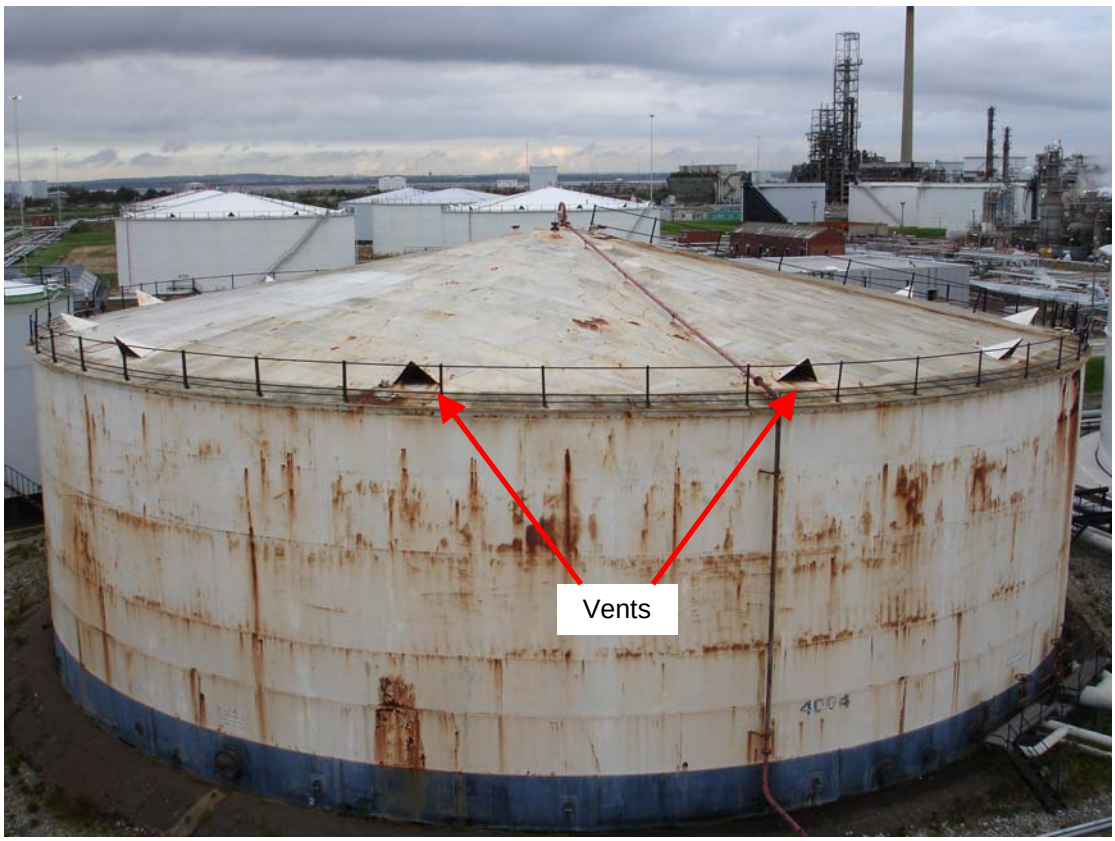

Figure 1 Fixed roof tank with vents (FRV)

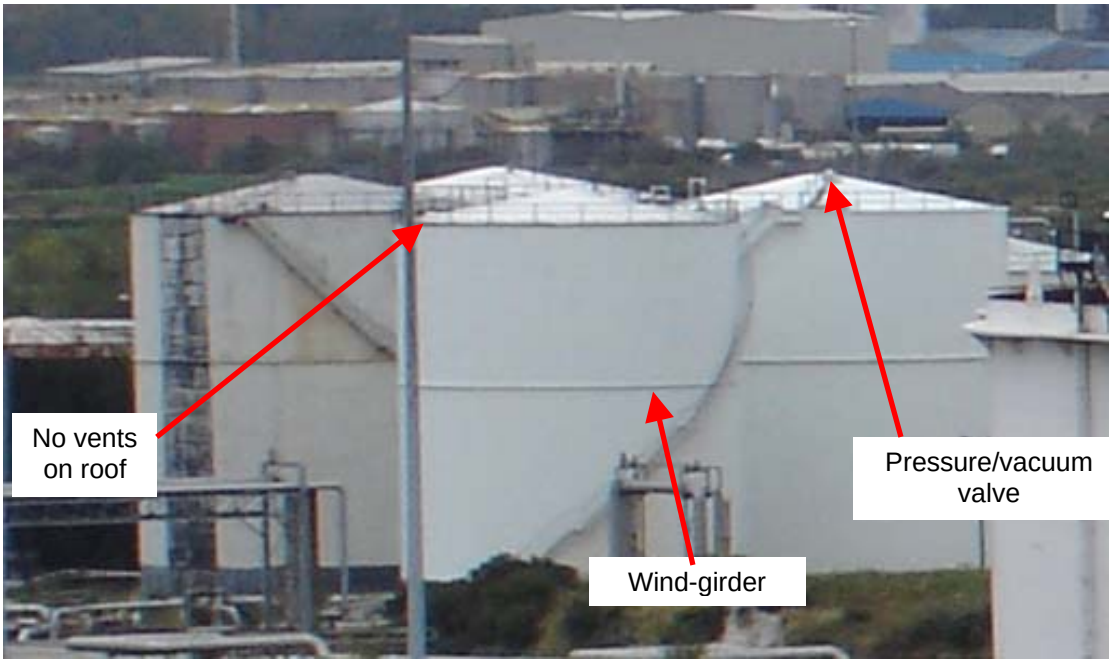

Figure 2 Fixed roof tanks with pressure/vacuum valves (FRPVV's)

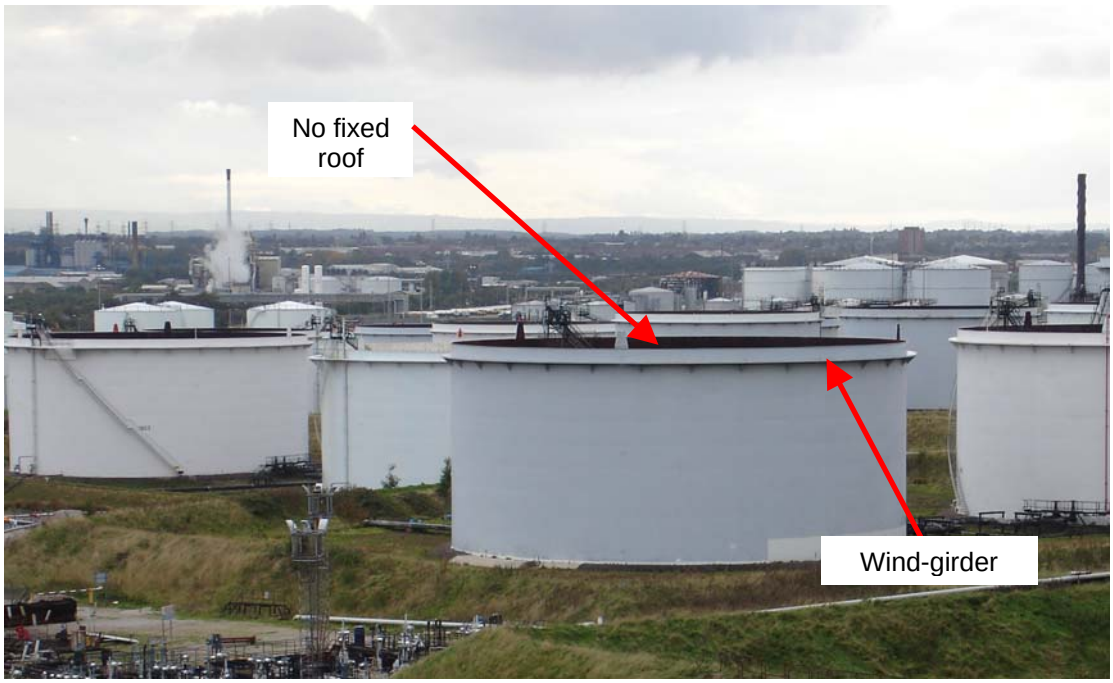

Figure 3 Floating deck (FD) tanks with no fixed roof

3 OVERFILLING RELEASE SCENARIOS

The release scenarios in an overfilling incident with FRV, FRPVV and FD tanks is likely to be different. Each class of tank is considered below and likely release scenarios are discussed.

3.1 FIXED ROOF TANK WITH VENTS (FRV)

Experience from Buncefield suggests that in an overfilling incident with an FRV tank the liquid will flow out of the roof vents, down the sloping roof and hit the deflector plate (shown in Figure 4). This angled plate is designed for use in fire situations to deflect water pumped onto the roof of the tank onto the sidewalls. In an overfilling incident, part of the liquid released through the roof vents will be directed onto the sidewalls. If the flow rate is sufficiently high, part of the flow will overtop the deflector plate and form a free spray (see Figure 5). If a wind-girder is present (as shown, for example, in Figure 2), the liquid flowing down the sidewalls will impinge onto this obstruction and form a secondary spray (Figure 6).

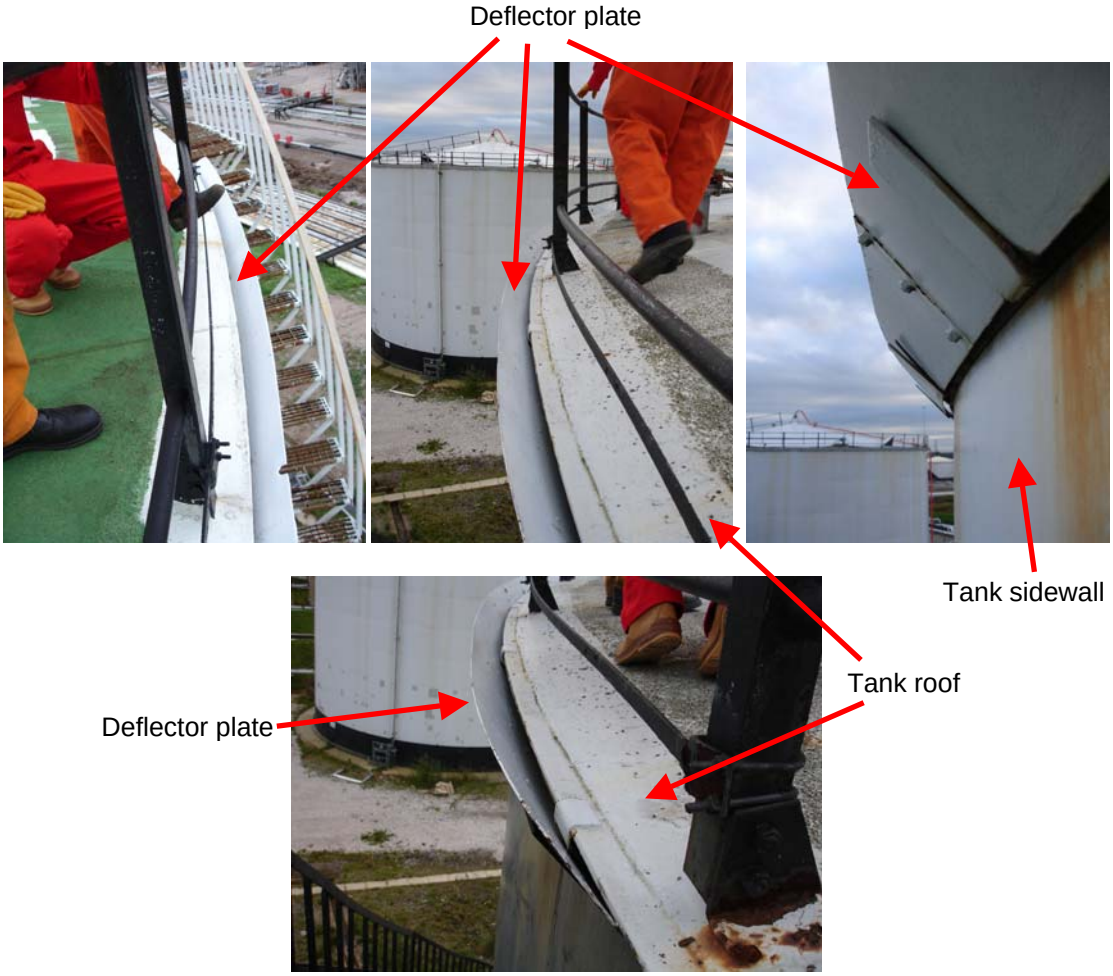

Figure 4 Several views of the deflector plate fixed around the perimeter of a fixed-roof tank

Figure 5 Photos of overfilling experiments from a section of a fixed roof tank showing liquid spilling over the deflector plate.

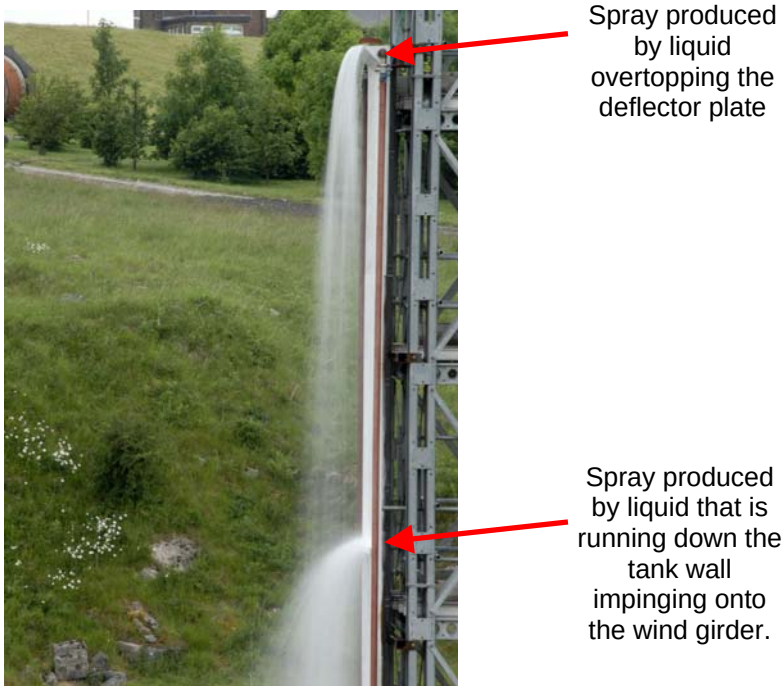

Figure 6 An overfilling experiment showing a section of the tank wall and the liquid sprays produced by overtopping of the deflector plate and impingement on the wind-girder.

3.2 FIXED ROOF TANK WITH PRESSURE/VACUUM VALVE (FRPVV)

When the fixed roof is fitted with a pressure/vacuum (p/v) valve, the cross-sectional area available for free liquid flow out of the tank is limited. The p/v valve is sized to allow the passage of air or vapour into or out of the tank to equalize pressures when the tank is filled or emptied. The orifice of the valve is not designed for liquid flow. In an overfilling incident, because of the limited flow of liquid through the valve, the pressure inside the tank is likely to build up. This may result in a pressurised liquid spray from the valve. Since the tank is not designed to hold liquid under significant pressure, it is likely to fail structurally. Tanks are designed to have their weakest point around the upper rim, where the sloping tank roof joins the sidewalls. An example of the likely result of a structural tank failure is shown in Figure 7. Since p/v valves are usually located near the top of the sloping roof, when the tank fails it will be nearly completely full of liquid with relatively little vapour under pressure. Since the liquid is essentially incompressible, once the crack opens the pressure will very quickly drop within the tank and the crack is unlikely to grow very large. To begin with there will be a head of liquid above the crack (that stored within the sloping roof of the tank) which may produce an initial peak in release rate before it declines to match the pumping rate into the tank. The flow will consist of a high-mass-density spray from the split into the bund.

Figure 7 Photo of a fixed-roof tank that has failed around the upper rim.

3.3 FLOATING DECK (FD) TANK WITH NO FIXED ROOF

Floating deck tanks with no fixed roofs have substantial wind-girders around the circumference near the top of the tank for structural rigidity (Figures 8a-c). According to Shell standards, the wind girder should be at least 600 mm wide. In many cases, the wind-girder serves a dual purpose as an access footway around the top perimeter of the tank. There are often small holes in the footway to drain water from rainfall, but these are only relatively small (typically around 10mm in diameter) and widely spaced so that the footway is nearly all solid (Figure 9).

In an FD tank overfilling incident, liquid could be released around the entire perimeter of the tank. It is unclear whether the floating deck would rise up and float on top of the liquid level or would become stuck at some point inside the tank, perhaps on the access bridge (see Figure 8b). If the floating deck is obstructed and unable to move further, it is likely that liquid will flow past the seals around its perimeter. Once the liquid level reaches the upper rim of the tank, it will start to flow over the edge of the tank, first onto the wind-girder and then from the edge of the wind girder into free space, forming a free-falling curtain spray. There may be some small differences in level around the upper rim of the tank (this aspect of tank design is not controlled to strict tolerances) so there could be flow preferentially around a low area rather than an equally distributed spray around the whole tank perimeter.

a.) FD tank with 3 wind girders

b.) FD tank showing access bridge

Figure 8a and 8b FD tanks with different wind-girder designs. The wind-girder around the tank on the left also acts as an access walkway around the tank perimeter.

Figure 8c Another FD tank with different wind-girder design.

Figure 9 View from the walkway around the top of an FD tank showing the floating deck towards the top of its travel.

3.4 SUMMARY

The sketches shown in Figure 10 summarise the likely mode of liquid release for the three tank types, with the liquid shown in blue.

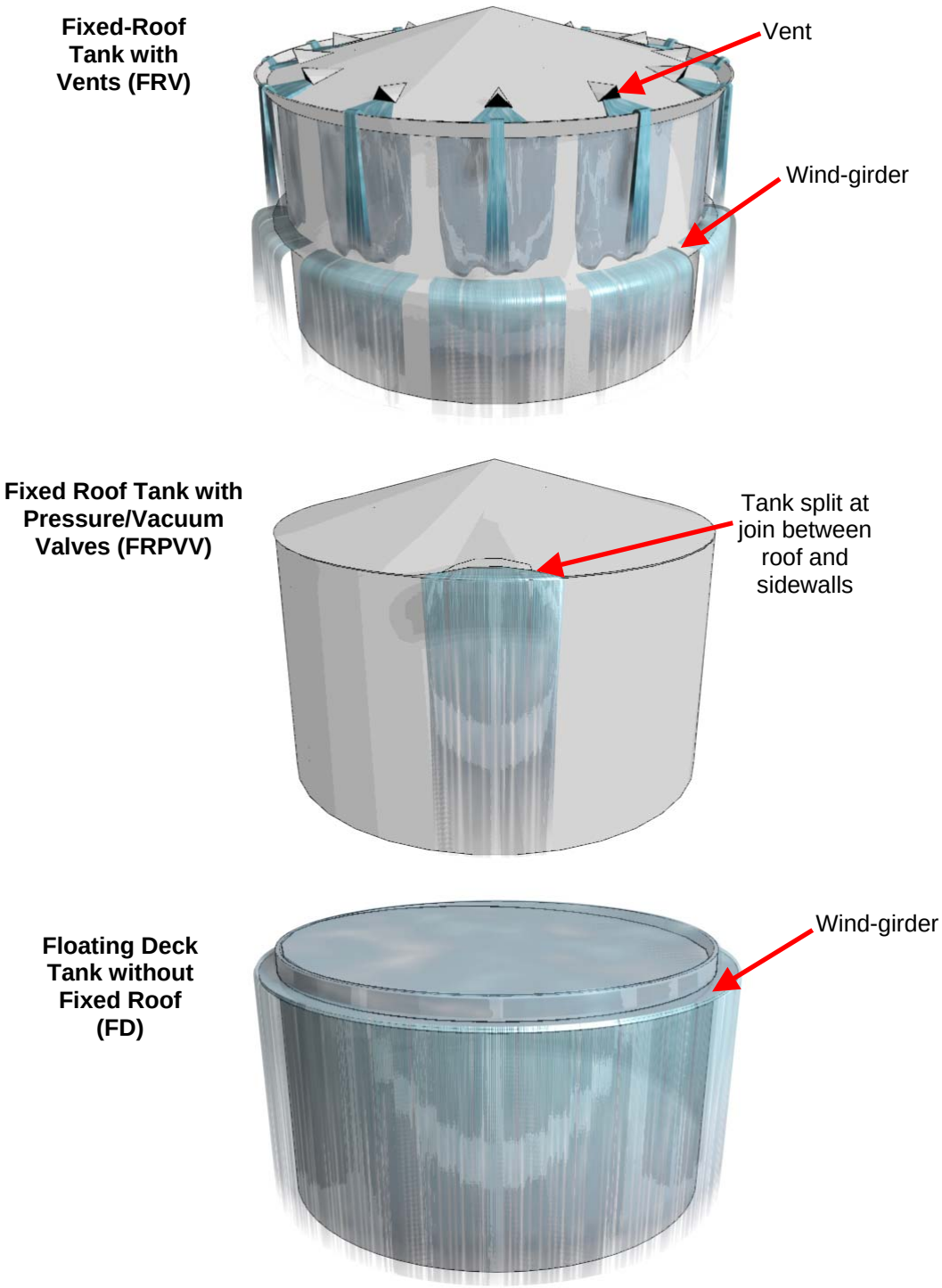

Figure 10 Sketches of the likely release scenarios from FRV, FRPVV and FD tanks

4 COMPUTATIONAL MODELLING OF OVERFILLING RELEASES

A number of CFD simulations have been undertaken to help understand the main factors affecting the production of vapour from a tank-overfilling incident. Section 4.1 documents some initial calculations that have used a simple two-dimensional model to examine the effect of spray mass density and droplet size on the amount of air entrained into a spray. Subsequent calculations, documented in Sections 4.2 to 4.6, have modelled more realistic three-dimensional release scenarios with the tank surrounded by bund walls. Table 1 provides an index of these simulations. In Section 4.2, the effect of the bund shape and the presence of a secondary tank on the vapour cloud are examined. Section 4.3 studies the sensitivity of predictions to the width of the spray, Section 4.4 examines the affect of spray droplet sizes, Section 4.5 different spray distributions and Section 4.6 the effect of a porous obstacle just outside the bund walls. All of these simulations ignore any vapour produced by evaporation from the pool of liquid within the bund, which is addressed in Section 4.7. Section 4.8 provides a summary of the CFD work and identifies the relative importance of the various parameters.

The CFD simulations are expected to provide qualitatively correct trends but, due to the uncertainties associated with spray formation and turbulence, they should not be taken as providing quantitatively accurate values for each specific scenario. For background information on the computational methods used and the level of uncertainty in spray calculations, see the recent validation study by Gant *et al*. [7].

The computational domain size used in most of the calculations was very large (up to 200 × 300 × 30 metres). Consequently, the computational grids used were of the order of 500,000 nodes and each simulation typically took around one week to compute. Standard best-practice CFD procedures such as grid-dependence and droplet-count sensitive studies have not yet been undertaken.

Table 1 Summary of three-dimensional CFD tank release calculations

Case	*General Description*	*Spray Release Area Around Tank Perimeter*	*Initial Mass Flow Density of Spray Release (kg/s/m^2)*	*Approximate Spray Width Close to the Ground (m)*	*Droplet Characteristics*	*See Section*
1	Bund wall close to tank	120˚	20.0	1.0	Monosized 2mm	4.2
2	Bund wall further from tank	120˚	20.0	1.0	Monosized 2mm	4.2
3	Sloping bund wall	120˚	20.0	1.0	Monosized 2mm	4.2
4	Adjacent secondary tank	120˚	20.0	1.0	Monosized 2mm	4.2
5	Narrow spray	120˚	4.0	2.5	Rosin-Rammler, δ = 2.21mm, γ = 1.5	4.3
6	Medium width spray	120˚	4.0	4.5	Rosin-Rammler, δ = 2.21mm, γ = 1.5	4.3, 4.4, 4.5, 4.6
7	Wide spray	120˚	4.0	5.5	Rosin-Rammler, δ = 2.21mm, γ = 1.5	4.3
8	Very wide spray	120˚	4.0	8.0	Rosin-Rammler, δ = 2.21mm, γ = 1.5	4.3
9	Fine spray droplets	120˚	4.0	4.5	Rosin-Rammler, δ = 1.105mm, γ = 1.5	4.4
10	Large spray droplets	120˚	4.0	4.5	Rosin-Rammler, δ = 3.315mm, γ = 1.5	4.4
11	Droplet breakup modelled	120˚	4.0	4.0	Rosin-Rammler, δ = 2.21mm, γ = 1.5	4.4
12	Multiple sprays	8 × 15˚	4.0	3.5	Rosin-Rammler, δ = 2.21mm, γ = 1.5	4.5
13	Continuous 360˚ spray	360˚	1.3	4.0	Rosin-Rammler, δ = 2.21mm, γ = 1.5	4.5
14	Porous blockage around tank	120˚	4.0	4.5	Rosin-Rammler, δ = 2.21mm, γ = 1.5	4.6

4.1 PRELIMINARY TWO-DIMENSIONAL CALCULATIONS

Figure 11 shows a schematic of a circular tank filling with liquid. The volume flow rate, Q, of liquid pumped into the tank causes the liquid level to rise with velocity V, such that:

$$Q = VA = V\pi r^2 \tag{1}$$

The perimeter length of the tank is given by $L = 2\pi r$. Assuming that a release takes place uniformly around the perimeter, the volume flow rate of liquid released from the tank per unit perimeter length is then:

$$\frac{Q}{L} = \frac{V\pi r^2}{2\pi r} = \frac{1}{2}Vr \tag{2}$$

The above equation provides a simple estimate of the volume flow rate of liquid released from floating deck tanks where liquid spills evenly over the entire perimeter of the tank. For typical tanks, the velocity is likely to range between 0.5 and 5.0 metres/hour with a radius of between 10 and 25 metres. Table 2 summarises the likely spread in Q/L values for this scenario.

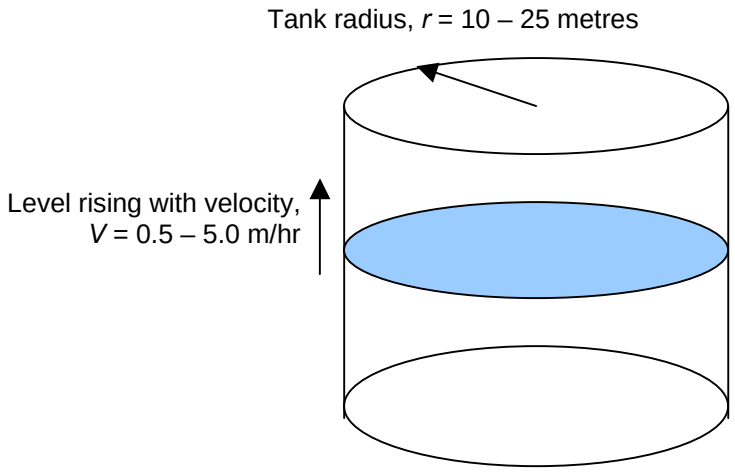

Figure 11 Schematic of filling tank showing typical tank filling rates and tank radii

Table 2 Summary of tank overfilling parameters

	Liquid level rising rate (m/hr)	*Tank radius (m)*	*Release rate per unit perimeter length, Q/L (m^3/s/m)*
Low	0.5	10	0.69
High	5.0	25	17.4

CFD simulations have been undertaken for an idealised model of the floating-deck tank overspill configuration (Figure 12). The idealised flow is two-dimensional and for the purposes of the present study the domain is only 1 metre wide. Four test cases covering the range of release conditions have been considered (Table 3). The sprays are released with droplets of a specified initial diameter and fall through the air under gravity. Droplet evaporation is not modelled. Figure 13 shows the development of the flow behaviour over the first 38 seconds from the droplets being released[1]. The droplets entrain air as they fall and drive air currents. The Coanda effect causes the air flow to be sucked against the side of the tank, leaving a small flow recirculation immediately beneath the wind-girder.

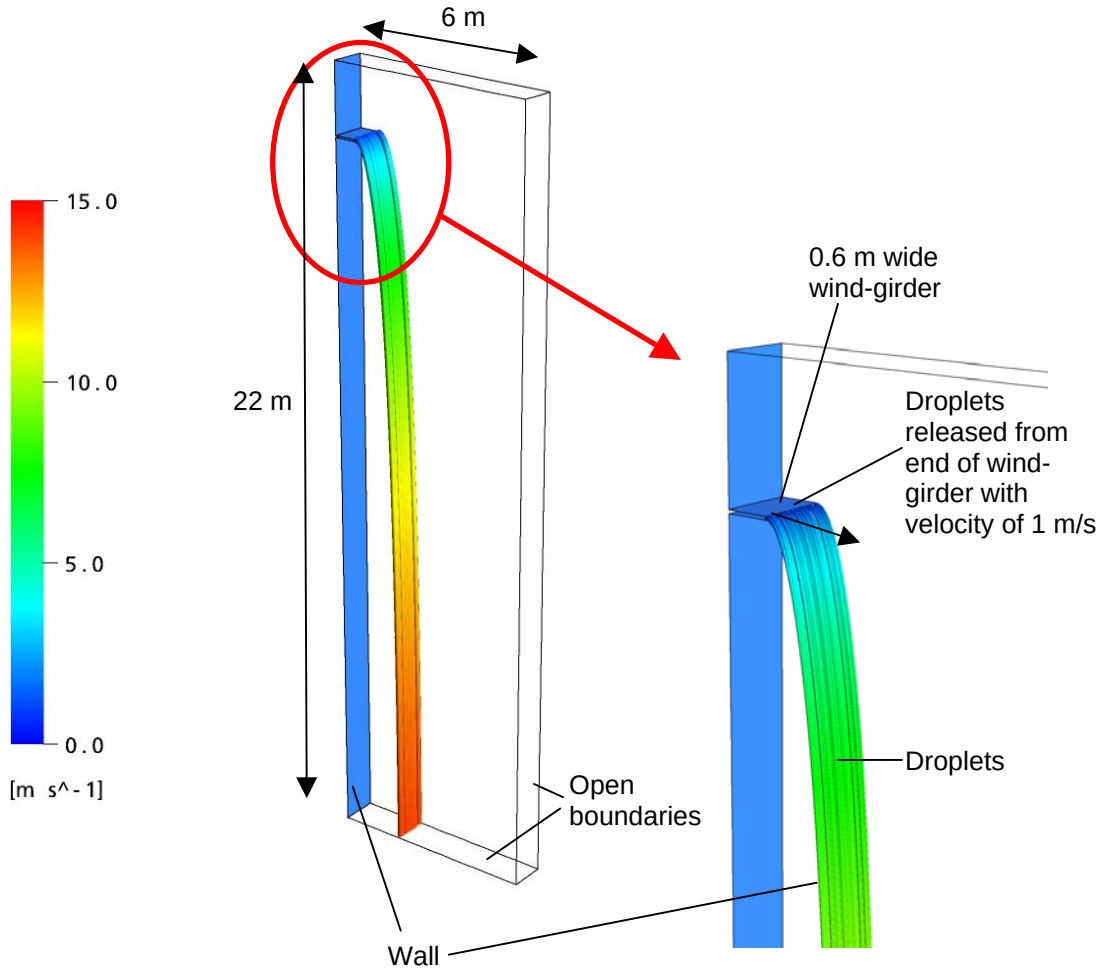

Figure 12 Two-dimensional spray arrangement used in the CFD simulations. Droplet trajectories are coloured the magnitude of their velocity.

[1] *Images between 20 and 38 seconds are omitted intentionally as they are identical.*

Table 3 Summary of mass release rates used in the CFD tests

Case	*Release rate per unit perimeter length, Q/L (m^3/s/m)*	*Mass flow rate per unit perimeter length (kg/s/m)*
1	0.69	0.48
2	6.3	4.3
3	11.8	8.1
4	17.4	11.9

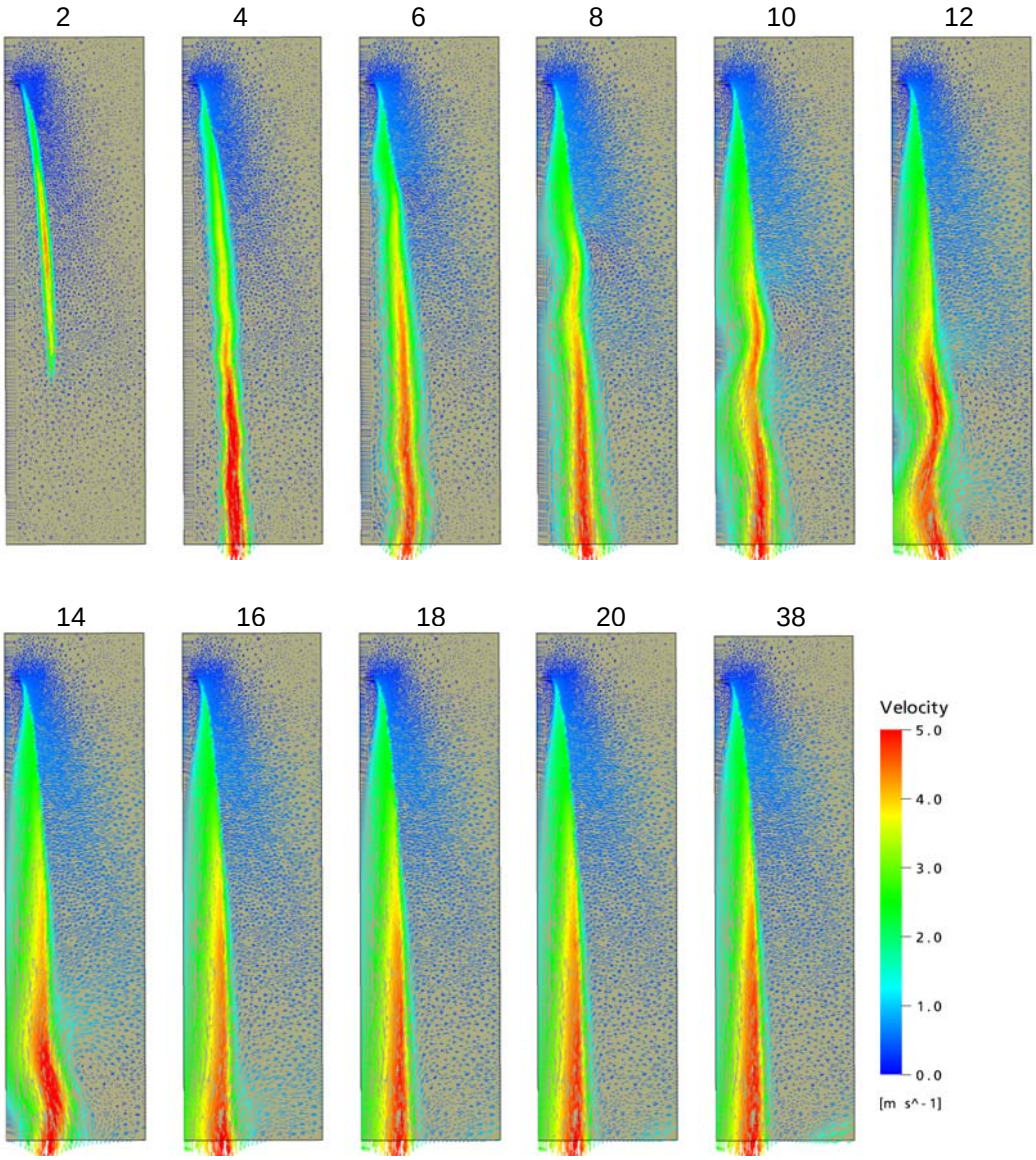

Figure 13 Development of the air/vapour flow over time. Vapour velocity vectors are coloured with velocity magnitude. Times shown are in seconds.

Figure 14 shows the variation in entrained air mass flow rate as a function of height. This is calculated by integrating over horizontal planes at different heights in the CFD model. Below a height of 2 metres the entrainment rates should be interpreted with care due to the influence of the lower boundary on the solution. The graphs show that the amount of air entrained increases almost linearly with distance fallen. For the releases considered here, the higher liquid mass flow rates lead to higher entrainment rates. An order of magnitude increase in the liquid mass flow rate per unit perimeter length from 0.48 to 4.3 kg/s/m roughly doubles the amount of entrained air, from 4.6 to 10.2 kg/s at the 5-metre position. As the mass of liquid released is increased still further, the increase in the amount of air entrained becomes less significant. This behaviour is consistent with a simple physical model of air entrainment. For sprays with low mass flow densities only a small amount of air is entrained. As the spray becomes more dense so the droplet drag force operates over a larger effective area and the amount of air entrained increases. However, this trend does not continue indefinitely. For very dense sprays, the air within the spray is travelling at practically the same velocity as the droplets, so by increasing the number of droplets in a given space the drag force is increased further by only a small amount.

The entrained air flow-rates for different initial droplet sizes are given in Figure 15. The four results shown are for two monodisperse sprays (with 2 mm and 5 mm diameter droplets) and two variable-droplet-diameter sprays. The variable droplet diameters arise due to aerodynamic breakup of the droplets. Initially the droplets are released with a diameter of either 10 mm or 20 mm and as they fall through the air, they fragment due to aerodynamic instability. The Reitz-Diwakar breakup model was used with a surface tension coefficient of 21 dynes/cm, characteristic of petrol. There is only a relatively modest influence on the amount of entrained air due to differences in the droplet sizes (Figure 15). The predicted size of droplets resulting from breakup is shown in Figure 16. After falling 4 metres, the droplets with initial diameters of 10 mm and 20 mm stabilize at between 4 and 5 mm in size.

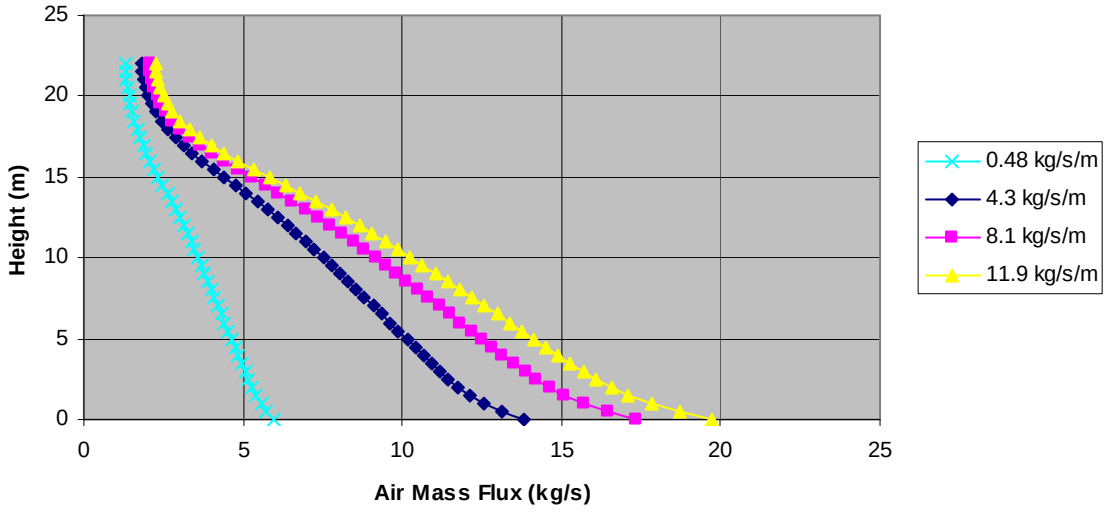

Figure 14 Mass flow rates of entrained air for different release rates of liquid. The wind-girder is at a height of 20 metres. In all four cases, the droplets are 5 mm in diameter.

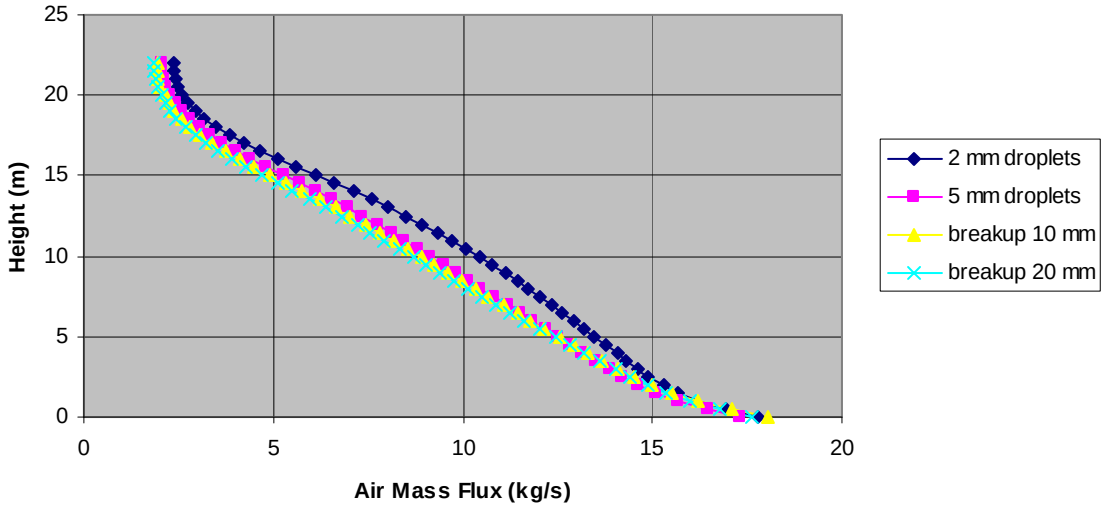

Figure 15 Mass flow rates of entrained air for different droplet sizes. In all four cases, the mass flow rate of liquid released is 8.1 kg/s/m.

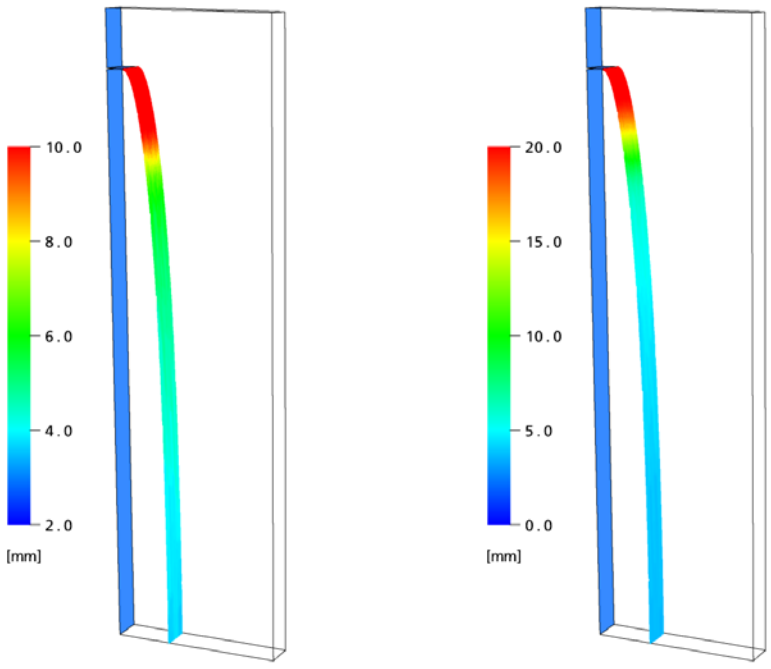

a.) Initial droplet size of 10mm

b.) Initial droplet size of 20mm

Figure 16 Predicted droplet diameters for two sprays with different initial droplet sizes. In both cases, the mass flow rate of liquid released is 8.1 kg/s/m. Note the difference in scales between the two plots.

4.2 BUND SHAPE/LOCATION AND TANK PROXIMITY

Three-dimensional CFD simulations were undertaken for four different tank releases in which the shape and location of the bund wall was either changed or a second tank was added in close proximity to the overflowing tank. The spray release conditions were identical in each case, only the geometry of the area surrounding the primary tank was changed. Figure 17 shows the CFD model of the primary tank, from where the release takes place. A summary of the modelled conditions is given below:

- Spray release from 1/3 of tank perimeter (120˚)
- Hexane droplets released with initial diameter of 2 mm and temperature of 15˚C
- Total liquid mass flow rate: 105 kg/s
- Initial horizontal momentum of droplets: 1 m/s
- Tank dimensions: diameter 25 m, height 15 m, 1:5 pitched roof
- Ambient conditions: zero wind speed, temperature 0˚C
- CFD simulations run for first 2 minutes of release

To simplify the CFD model, instead of simulating the release of a complex multi-component liquid mixture of petrol (composed of butane, pentane, hexane etc.) the liquid released was modelled as pure hexane. This should provide a reasonable approximation for the behaviour of petrol. The CFD model accounted for droplet evaporation and the associated heat transfer effects. Atmospheric conditions of 0˚C and nil-wind were chosen to match the conditions present in the Buncefield Incident. Rather than release a liquid sheet and model its fragmentation into filaments and droplets, the liquid was released as a spray composed of droplets of a given size. The droplets initial diameter of 2 mm is representative of the mean diameter observed in tank release experiments undertaken by HSL for the Buncefield Investigation [1-3]. The droplets were given an initial horizontal velocity such that their trajectory matched approximately the observed flow behaviour in the Buncefield experiments. When the droplets hit the floor of the bund they were removed from the simulation. Any vapour generated through evaporation from the liquid pool within the bund was ignored in the CFD model.

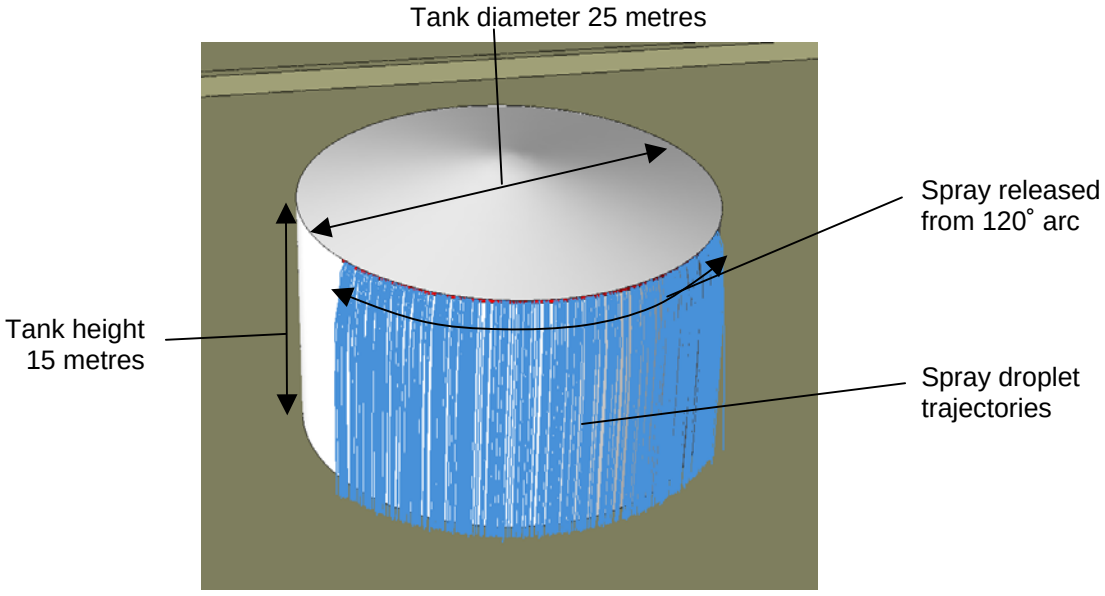

Figure 17 Tank spray release conditions

The four different cases tested are as follows:

Case 1. Bund wall close to tank
Case 2. Bund wall farther away from tank
Case 3. Sloping bund wall close to tank
Case 4. Two tanks close together

Three-dimensional views and cross-sections of each of these models are shown in Figure 18.

Figure 19 shows the vapour cloud produced by the spray releases 2 minutes after the liquid started flowing from the tank. The clouds shown are defined by a gas concentration iso-surface at the Lower Explosive Limit (LEL), which for hexane is 1.2% v/v. Colours indicate the distance from the cloud boundary to the nearest wall surface which in most areas is equivalent to the cloud depth. Cases 1 and 2, which both feature vertical bund walls, produce a similar shape of vapour cloud that extends a relatively short distance radially from the tank but further laterally along the width of the bund wall. When the bund wall is closer to the tank (Case 1), the vapour cloud spreads slightly more laterally than when the bund wall is further away from the tank. The sloping bund wall (Case 3) produces a vapour cloud of different shape that is shallower and extends much further radially away from the source. The lateral spread of the cloud in Case 3 is much less than for both Cases 1 and 2. The presence of the second tank in Case 4 produces a 'bow wave' of vapour around the side of the tank facing the release. After 2 minutes the cloud extends around the whole circumference of the second tank and flows over the bund wall on its far side.

None of the geometries considered appears to lead to significant re-entrainment of vapour into the sprays, at least within the first 2 minutes of the release. This can be seen more clearly in Figure 20, which shows the vapour concentrations on a cross-section through the flow. A notable feature of Figure 20 is the large circular cross-sectioned region of concentrated vapour immediately downstream of the bund wall in Case 2. This is produced as a consequence of the vapour rising in this region of the flow. Vapour velocity vectors and streamlines are shown in Figures 21 and 22 respectively, to help understand this flow behaviour.

In the CFD simulations, the spray droplets leaving the tank cascade vertically downwards and reach speeds of up to 10 m/s as they near the ground. This drives the vapour flow at around 6 m/s vertically downwards parallel to the tank wall. The vapour then impinges onto the floor of the bund and travels radially outwards from the base of the tank at around 5 m/s. As the vapour flow hits the bund wall it is projected vertically upwards. Part of the flow then falls back into the bund and part of it forms a large recirculation immediately downstream of the bund wall. It is this vertical velocity and flow recirculation which leads to the large, circular cross-sectioned region of vapour in Case 2 shown in Figure 20.

In Case 1, the bund wall is close to the tank and there is insufficient space for the vapour to flow horizontally across the bund floor before impinging onto the bund wall. Instead, the vapour impacts the bund wall at an angle from above (see the streamlines in Figure 22). This produces a much smaller flow recirculation in Case 1 than in Case 2. The sloping bund (Case 3) produces no flow recirculation and hence the cloud produced is much thinner and it travels faster away from the tank.

The amount of hexane vapour produced over time for the four cases studied is shown in Figure 23. After a few seconds, all of the cases produce almost identical hexane vapour production rates. This is confirmation of the lack of re-entrainment of vapour back into the sprays. If hexane-rich vapour was re-entrained back into the spray, the concentration gradient between the droplet surface and the surrounding gas would be reduced, lowering the evaporation rate and

producing a non-linear vaporization rate profile. The linear profiles in Figure 23 suggest that fresh air is continuously being fed into the sprays.

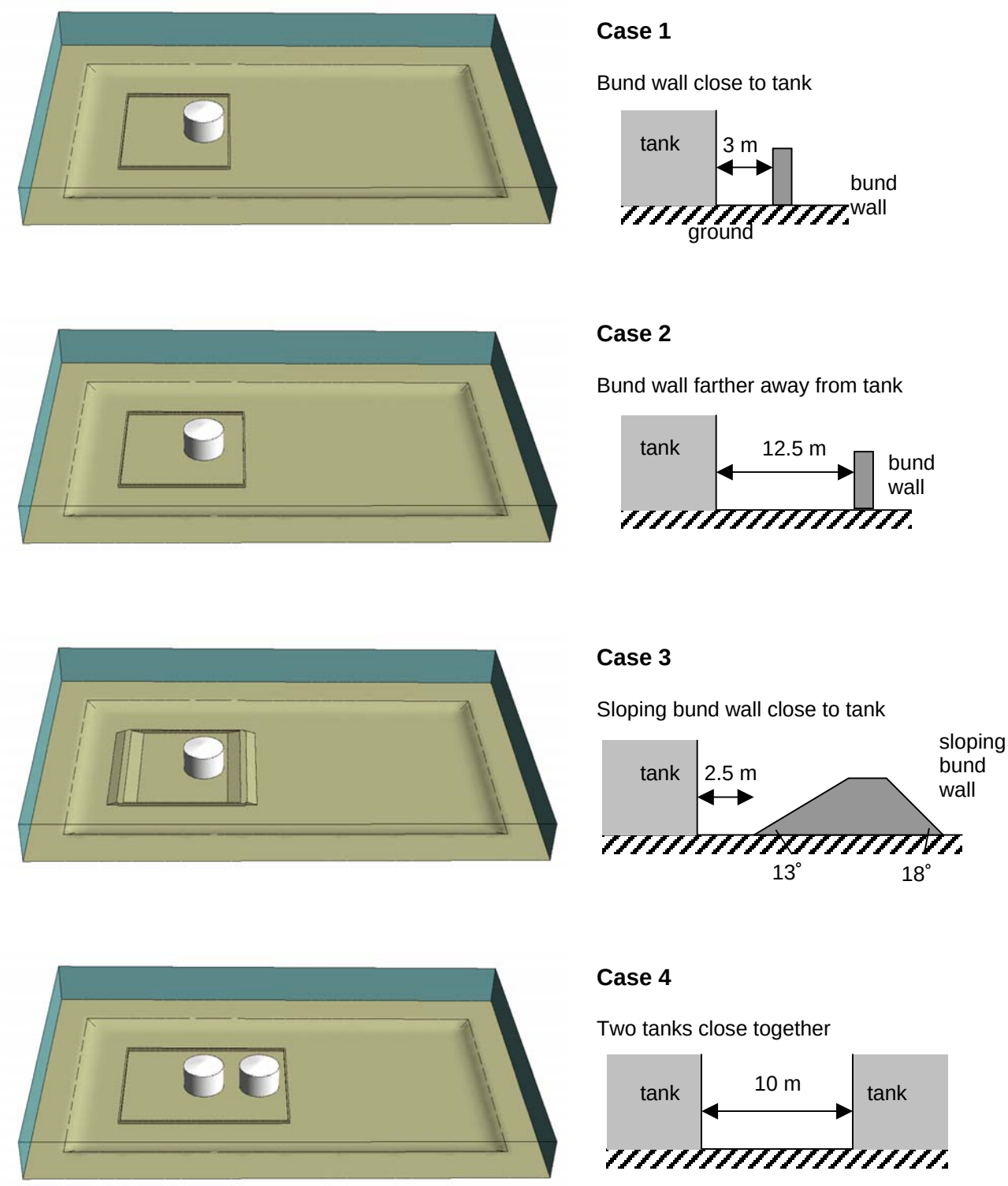

Figure 18 3D views of the CFD geometry and cross-sections of the tank/bund-wall configuration for the four test cases. In all cases, the bund wall is 1.8 metres high.

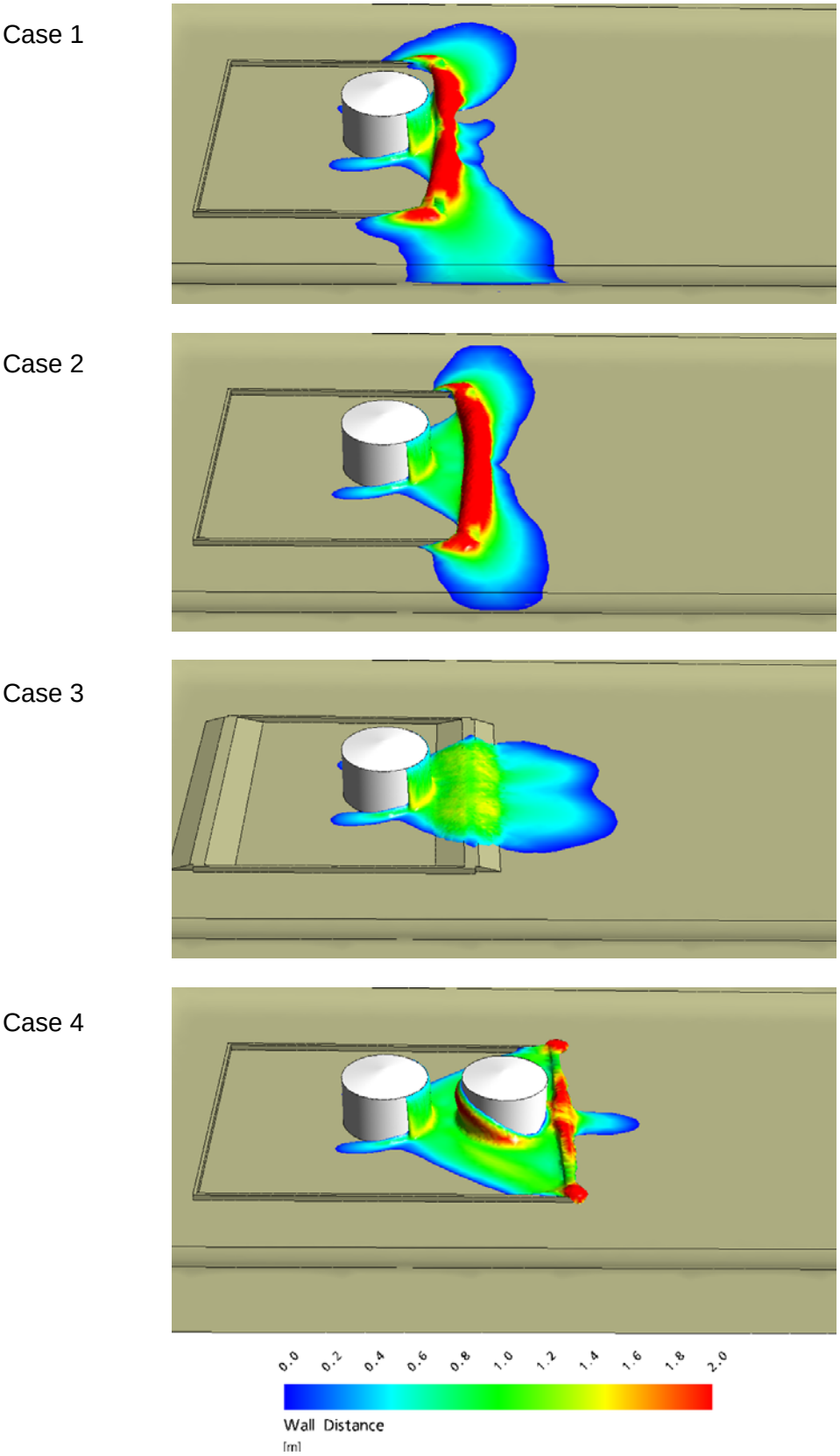

Figure 19 Vapour clouds defined using an iso-surface at the LEL coloured with wall distance (a similar measure to cloud depth) after 2 minutes from the start of the release for Cases 1 – 4.

Case 1

Case 2

Case 3

Case 4

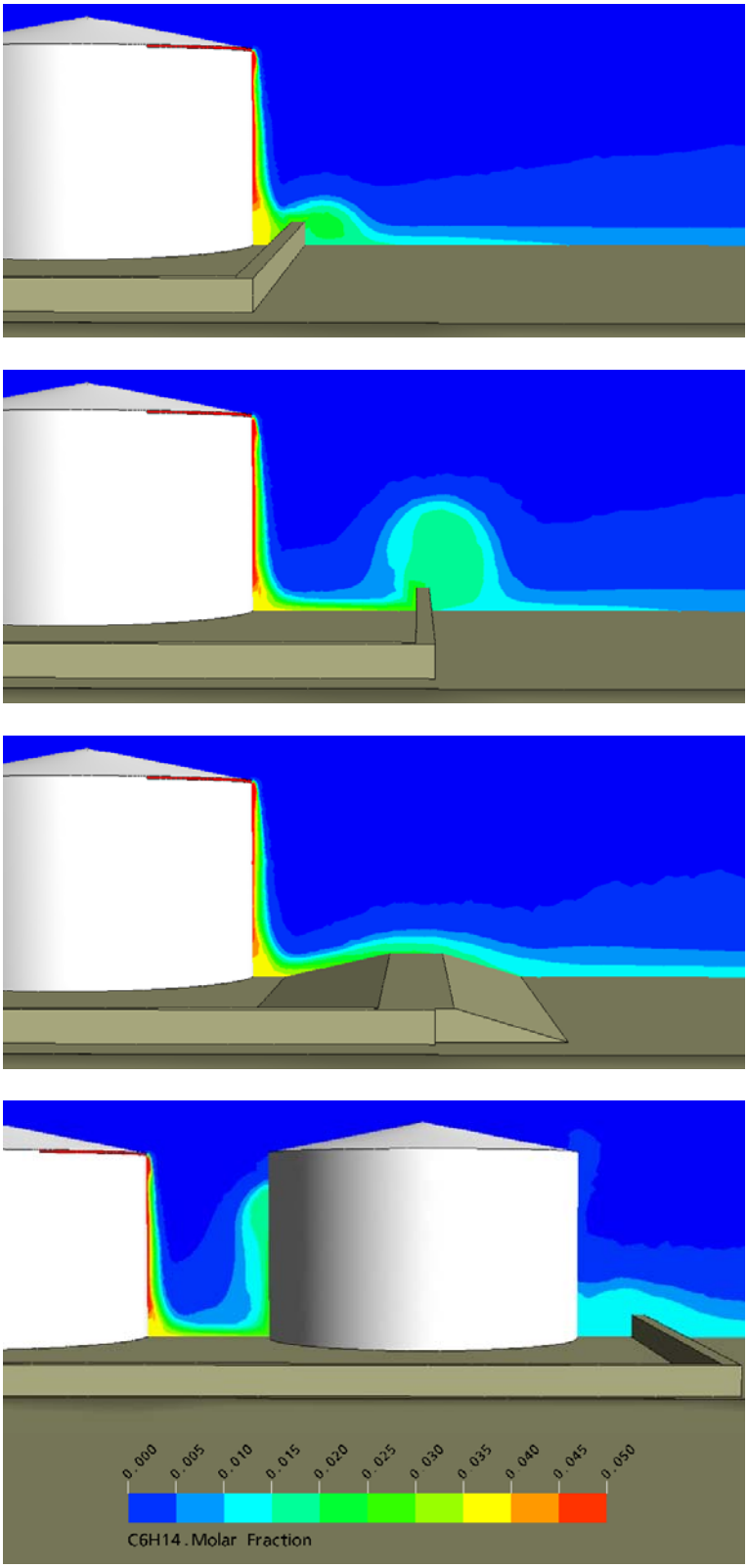

Figure 20 Contours of hexane vapour concentration on the vertical mid-plane for Cases 1 – 4.

Case 1

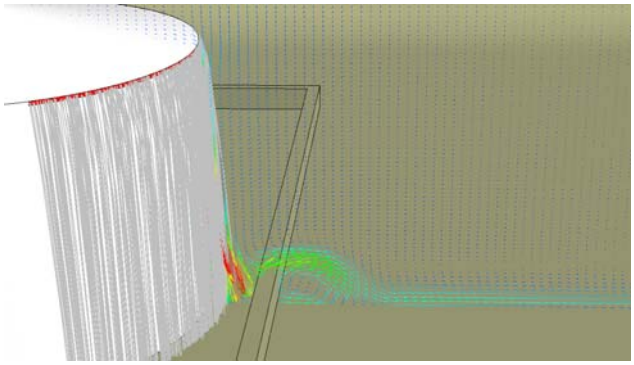

Case 2

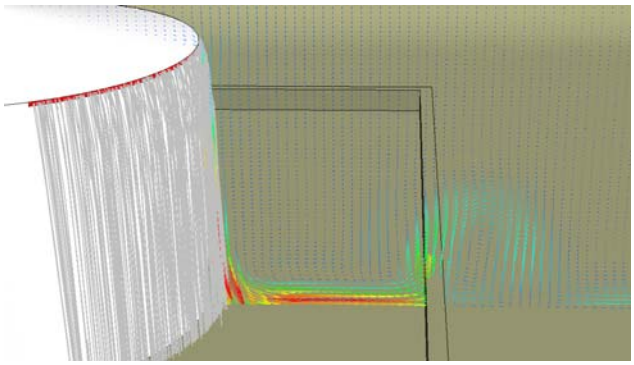

Case 3

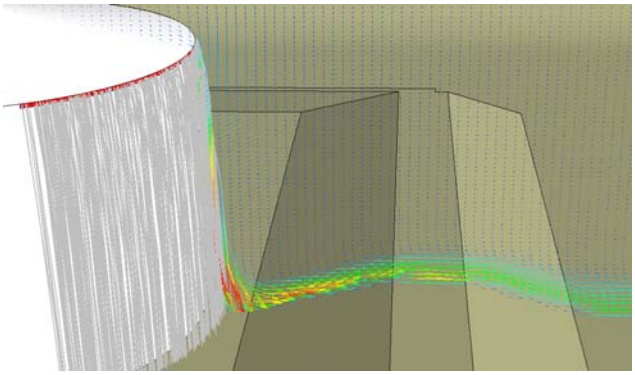

Case 4

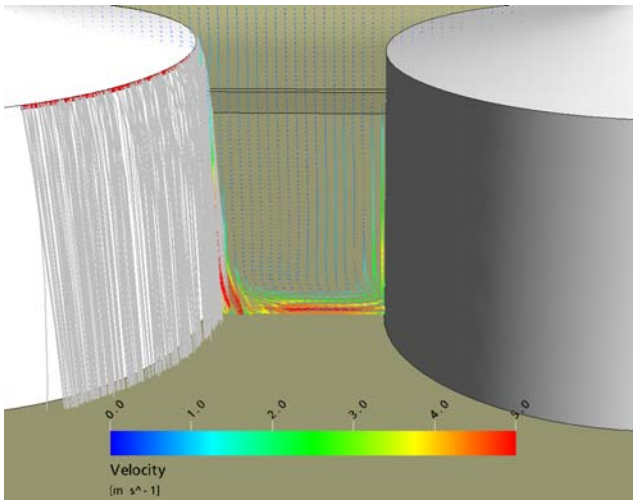

Figure 21 Velocity vectors coloured with velocity magnitude on the vertical mid-plane for Cases 1 – 4. The spray droplet trajectories are also shown in grey.

Case 1

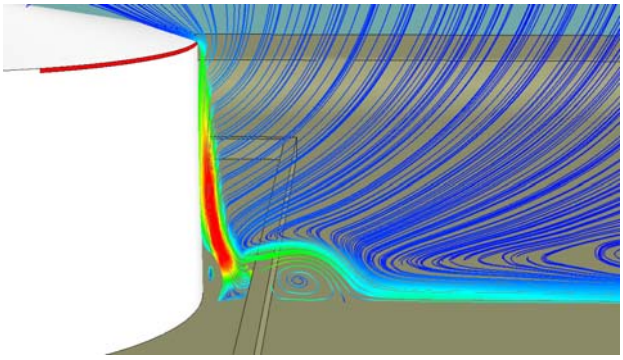

Case 2

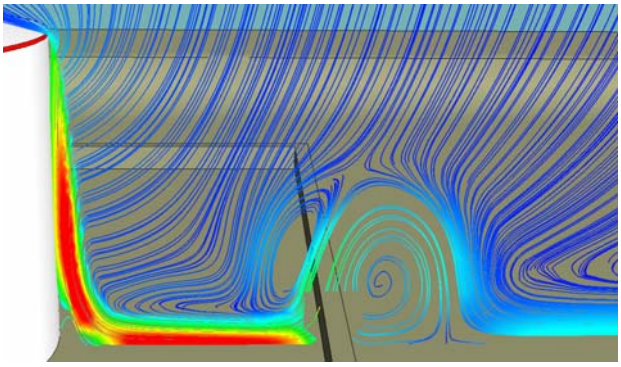

Case 3

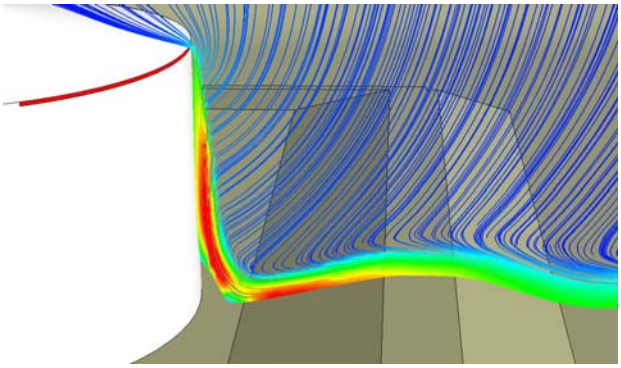

Case 4

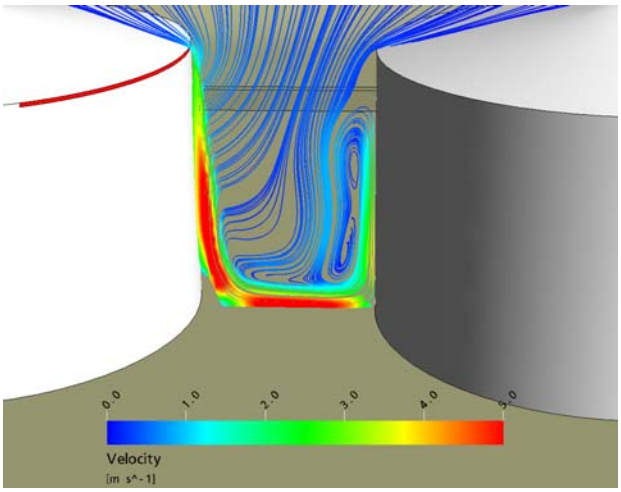

Figure 22 Streamlines coloured with velocity magnitude on the vertical mid-plane for Cases 1 – 4.

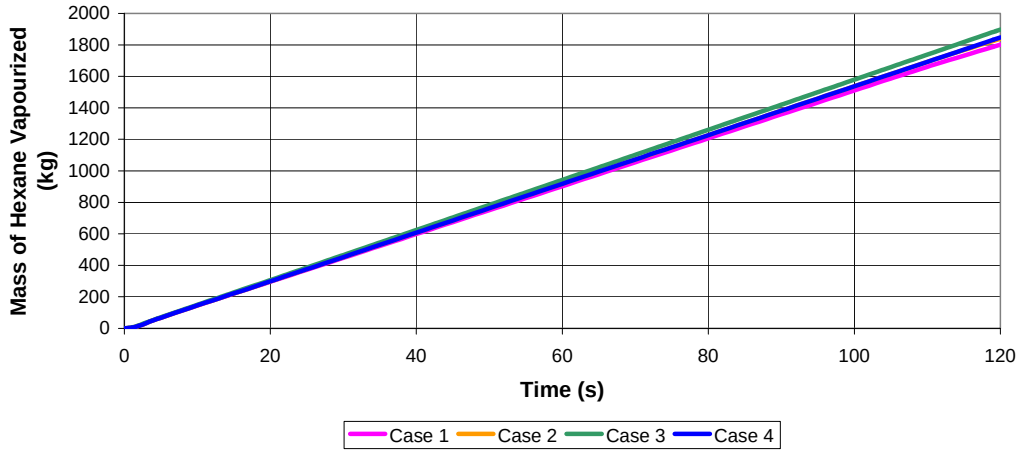

Figure 23 Total mass of hexane vaporized in the spray releases as a function of time

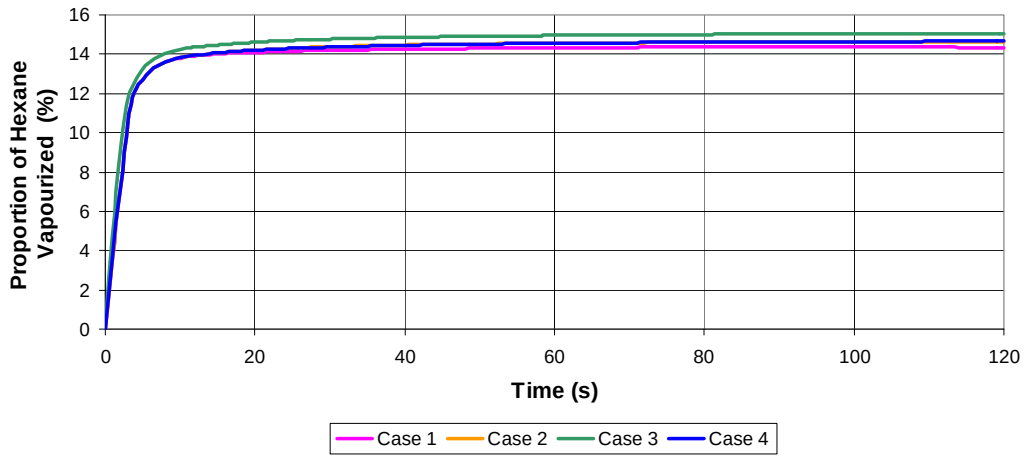

Figure 24 Percentage of hexane vaporized in the spray releases as a function of time

The hexane vapour production rate is shown expressed as a proportion of the total mass release rate of liquid in Figure 24. After an initial development time of around 20 seconds, the models predict that around 15% of the mass of liquid released evaporates.

Figure 25 shows the change in the volume of the vapour clouds for Cases 1–4 over time. The clouds are defined here as the volume enclosed by an iso-surface at the LEL. In all four cases the volume of the vapour clouds increases relatively quickly in the first 20 seconds. At around 25 seconds, the profile for Case 2 flattens for a few seconds before continuing to increase. This coincides with the vapour first reaching the bund wall and being thrown vertically upwards. After 2 minutes, the cloud volumes in these three cases are still increasing at a rate of tens of cubic-metres per second. In contrast, for the sloping bund (Case 3), the cloud volume reaches a maximum at around 25 seconds and thereafter remains relatively constant at around 4000 m^3. In this case, the cloud has reached the point where the dilution rate, determined by the mixing with the surrounding air, matches the rate at which the vapour is being produced. The vapour flowing

rapidly away from the sloping bund in a relatively thin layer appears to provide good conditions for enhanced dilution.

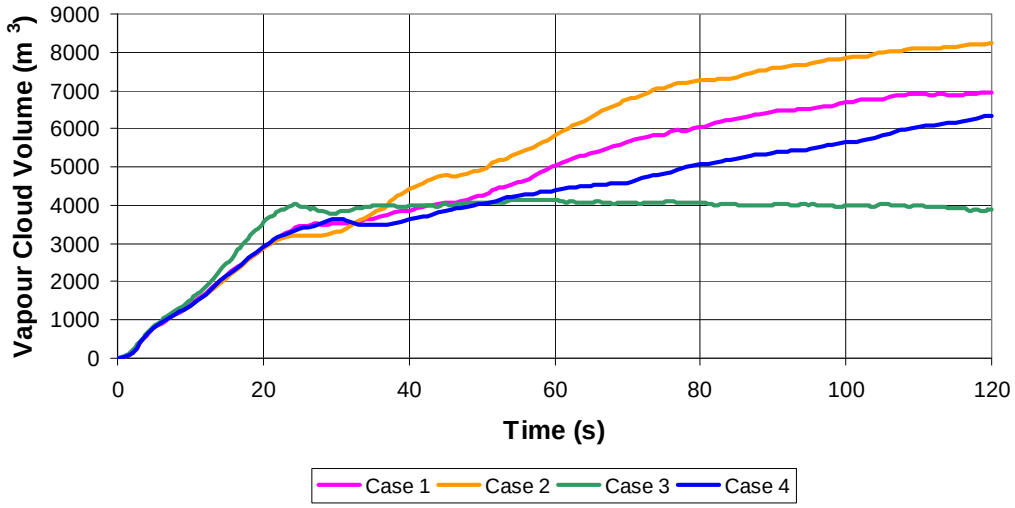

Figure 25 Growth of the vapour cloud volume over time. The cloud extent is defined by an iso-surface at the LEL.

In all cases the vapour concentrations are relatively low inside the bund, around 2 – 4% hexane by volume. In the Buncefield Incident, the burn damage indicated that the vapour concentration within the bund and in the area immediately adjacent to it was above stoichiometric at the time of the explosion [1-3]. Pure hexane is a reasonably representative model for the multi-component petrol mixture released at Buncefield. The stoichiometric and Upper Explosive Limit (UEL) concentrations for hexane are 2.2% and 7.5% v/v (Table 4).

Table 4 Flammability limits and stoichiometric ratios for common hydrocarbon compounds (from Harris [8])

Chemical Name	*Composition*	*Flammability Limits (% v/v)*		*Stoichiometric Concentration (% v/v)*
		Lower	*Upper*	
Butane	C_4H_{10}	1.9	8.5	3.1
Pentane	C_5H_{12}	1.5	7.8	2.6
Hexane	C_6H_{14}	1.2	7.5	2.2
Benzene	C_6H_6	1.4	7.1	2.7
Heptane	C_7H_{16}	1.2	6.7	1.9

To help explain why the vapour concentrations are relatively low in the CFD model, droplet temperatures are shown in Figure 26. As the liquid droplets fall through the air and evaporate, their temperature decreases due to the loss of latent heat. In the CFD model, the droplets are released with an initial temperature of 15°C and by the time they have reached the bund floor most of them have cooled to around -10°C. The air surrounding the tank has an initial temperature of 0°C. Two minutes after the start of the spray release, the temperature in the air

has risen to approximately 8°C in a very thin layer close to the tank wall (which is itself at 15°C) and in the main spray region where the droplets evaporate, the gas temperature is between -2°C and 1°C.

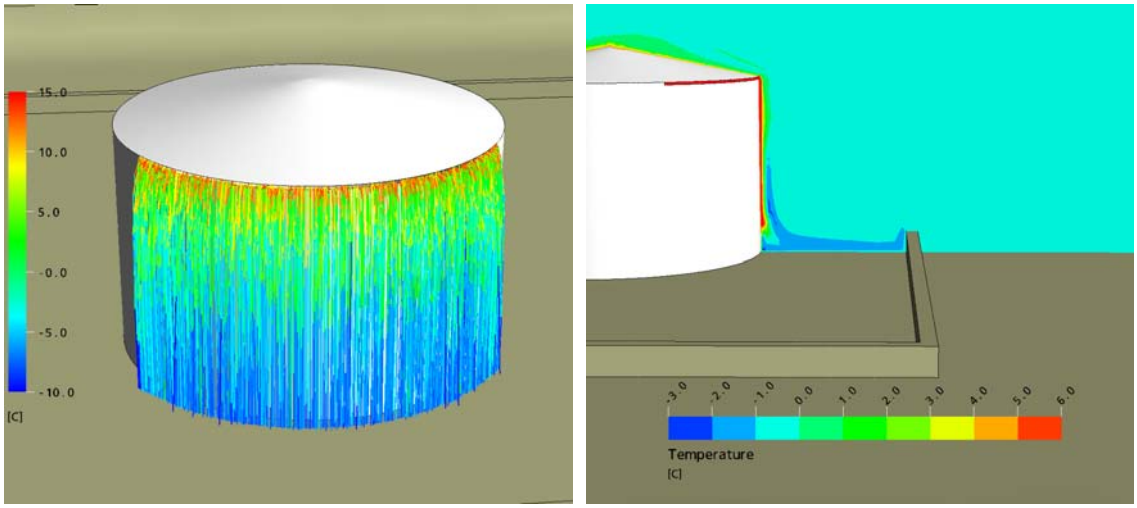

a.) Droplet temperatures

a.) Gas temperatures

Figure 26 Predicted temperatures for Case 2.

Evaporation of the droplets is driven by the concentration gradient between air and the droplets surface. At the surface of the droplets the vapour pressure is at the saturation condition. Once the vapour pressure in the air has reached this level, no further evaporation can take place. This therefore provides an upper limit on the concentration that can be present in the air. The saturation vapour pressure, P^{sat}, can be calculated from the Antoine equation:

$$P^{sat} = P_{ref} \exp\left(A - \frac{B}{T + C} \right) \tag{3}$$

where P_{ref} is standard atmospheric pressure and A, B and C are material-specific coefficients (for hexane: A = 20.75, B = 2708 K and C = -48.25 K). A plot of the saturation vapour pressure for hexane, expressed in terms of the vapour concentration, as a function of temperature is given in Figure 27. The maximum possible vapour concentration that is possible at temperatures between -2°C and 1°C is around 6% by volume. Since the droplets are passing through the air and may not have time to reach equilibrium conditions, it is reasonable to find that the mean vapour concentrations within the bund are only 2 – 4% v/v in the CFD simulations.

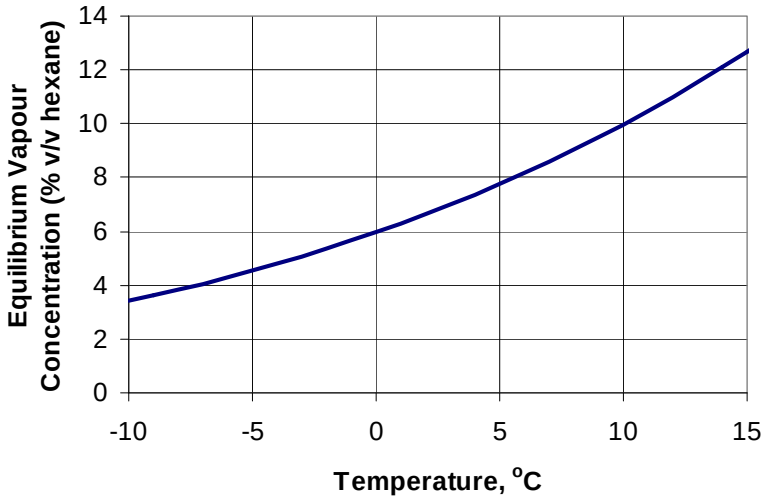

Figure 27 Equilibrium vapour concentration for hexane in air at atmospheric pressure

To examine the relationship between the vapour concentration and the saturation condition, the ratio of the vapour mole fraction, X, to the local saturation mole fraction, X^{sat} was calculated from:

$$\varphi = \frac{X}{X^{sat}} = \frac{X}{P^{sat} / P^{amb}} \tag{4}$$

where P^{amb} is the ambient pressure (101325 Pa), and P_A^{sat} is the saturation vapour pressure calculated from Antoine's equation using the local temperature. A value of $\varphi = 1$ would indicate that the vapour is saturated and $\varphi = 0$ that there is no vapour present. The resulting values of φ for Case 2 shows that the vapour is never fully saturated (Figure 28). The maximum value of φ is approximately 0.7, in a small region near the base of the tank. The vapour layer within the floor of the bund is at a concentration below $\varphi = 0.5$ and in the circular cross-sectioned region near the bund wall φ is less than 0.4.

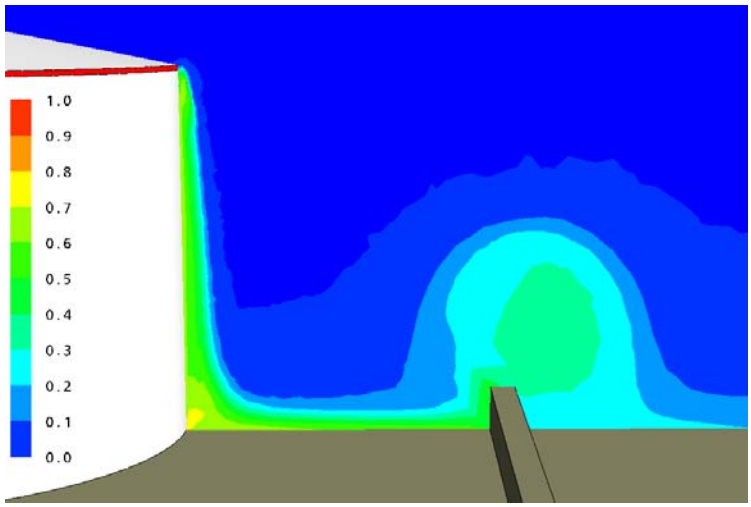

Figure 28 CFD results for Case 2 showing the ratio of the local vapour concentration to the local saturation concentration.

4.3 SPRAY CROSS-SECTIONAL AREA

The results presented in the previous section were based on a model of an overfilling release as a relatively thin, dense curtain spray falling from one-third of the tank perimeter. Close to the ground, the modelled spray was only around 1 metre wide (Figure 29). Experiments undertaken at HSL for the Buncefield Investigation (Figures 5 and 6) indicated that as the liquid droplets fell from the top of a tank, the spray widened due to droplet breakup, droplet-droplet collisions, turbulence and aerodynamic effects. At the base of the tank, the spray in the experiments was between 3 and 4 metres wide in the radial direction.

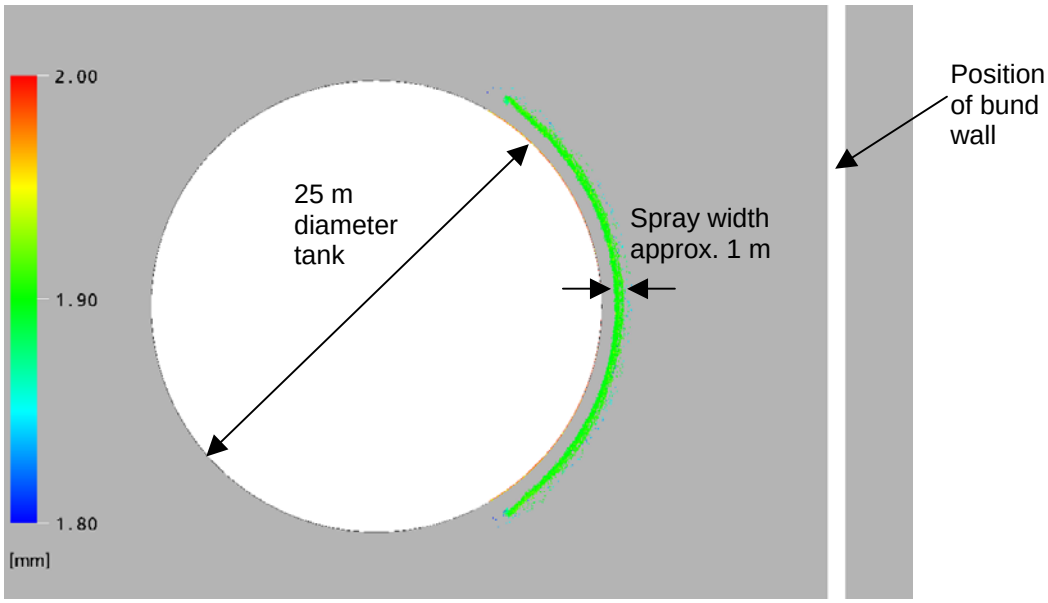

Figure 29 Horizontal section through the Case 2 CFD model at a height of 1 metre above ground level showing the position of spray droplets, coloured according to their diameter.

Four further CFD simulations were undertaken to produce a more realistic spreading of the spray. These used different initial droplet velocity profiles to obtain a range in droplet trajectories. The effects of droplet-droplet collisions, turbulent dispersion and breakup were not modelled. The droplets in these simulations were given an initial diameter determined using the Rosin-Rammler size distribution:

$$1 - \nu = \exp\left[-\left(D/\delta\right)^{\gamma}\right] \tag{5}$$

where ν is the fraction of the total liquid volume contained in droplets smaller than diameter D, δ is the Rosin-Rammler diameter and γ is a constant indicating the range of droplet sizes. A higher value of γ indicates that the spray is composed of more uniformly-sized droplets. If γ is infinite, the spray is 'monodisperse' (i.e. single-sized). A typical range of values for γ is between 1.5 and 3 and in the present study a value of 1.5 has been used. The volume-weighted number mean diameter of the spray has been chosen to be 2 mm, equivalent to a Rosin-Rammler diameter of 2.21 mm. Figure 30 shows the volume frequency distribution for this

spray. The Rosin-Rammler size distribution has previously been used in CFD simulations of fire-suppression sprinklers by Yoon *et al*. [9], Walmsley [10] and Chow & Fong [11].

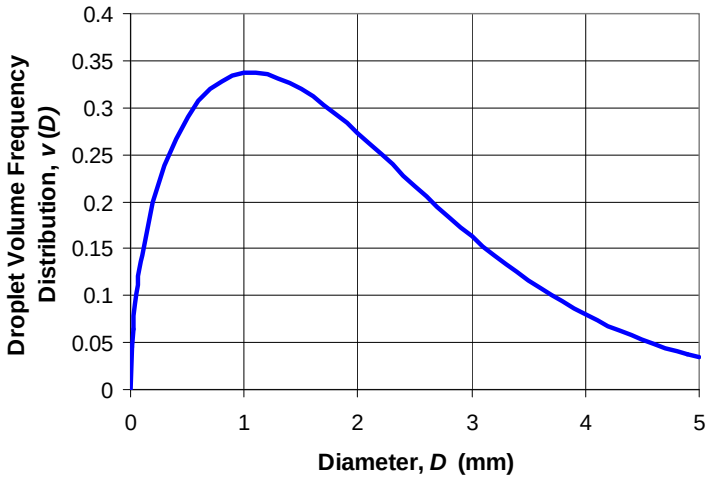

Figure 30 Rosin-Rammler size distribution

The four cases modelled, denoted Cases 5 – 8, used the same mass release rate as that used previously in Cases 1 – 4 (105 kg/s of hexane). The tank and bund geometry was identical to that used in Case 2, with the spray being released from a single 120º section of the tank rim. In an effort to reduce the overall computing time of the calculations, Cases 6 – 8 used a smaller overall computational domain size (120 × 140 metres instead of 200 × 300 metres used previously). To simulate the first two minutes of the release took around 5 days to compute, compared to the previous 9 days.

Figure 31 presents cross-sections through the computational domain showing side views of the spray trajectories from the four models. A plan view of the distribution of droplets produced by the modelled sprays is shown in Figure 32 and the spray widths 1 metre above ground level are summarized in Table 5. The four cases provide a reasonable range in spray widths: Case 5 is narrower than the spray generated in the HSL experiments, Case 6 is roughly similar to the experiments and Cases 7 and 8 are wider than the experiments. The spray in Case 8 is around three times the width of that in Case 5.

Table 5 Approximate radial widths of the modelled sprays 1 metre above the floor of the bund for Cases 5 – 8.

Case	*Approx. Spray Width (m)*
5	2.5
6	4.5
7	5.5
8	8.0

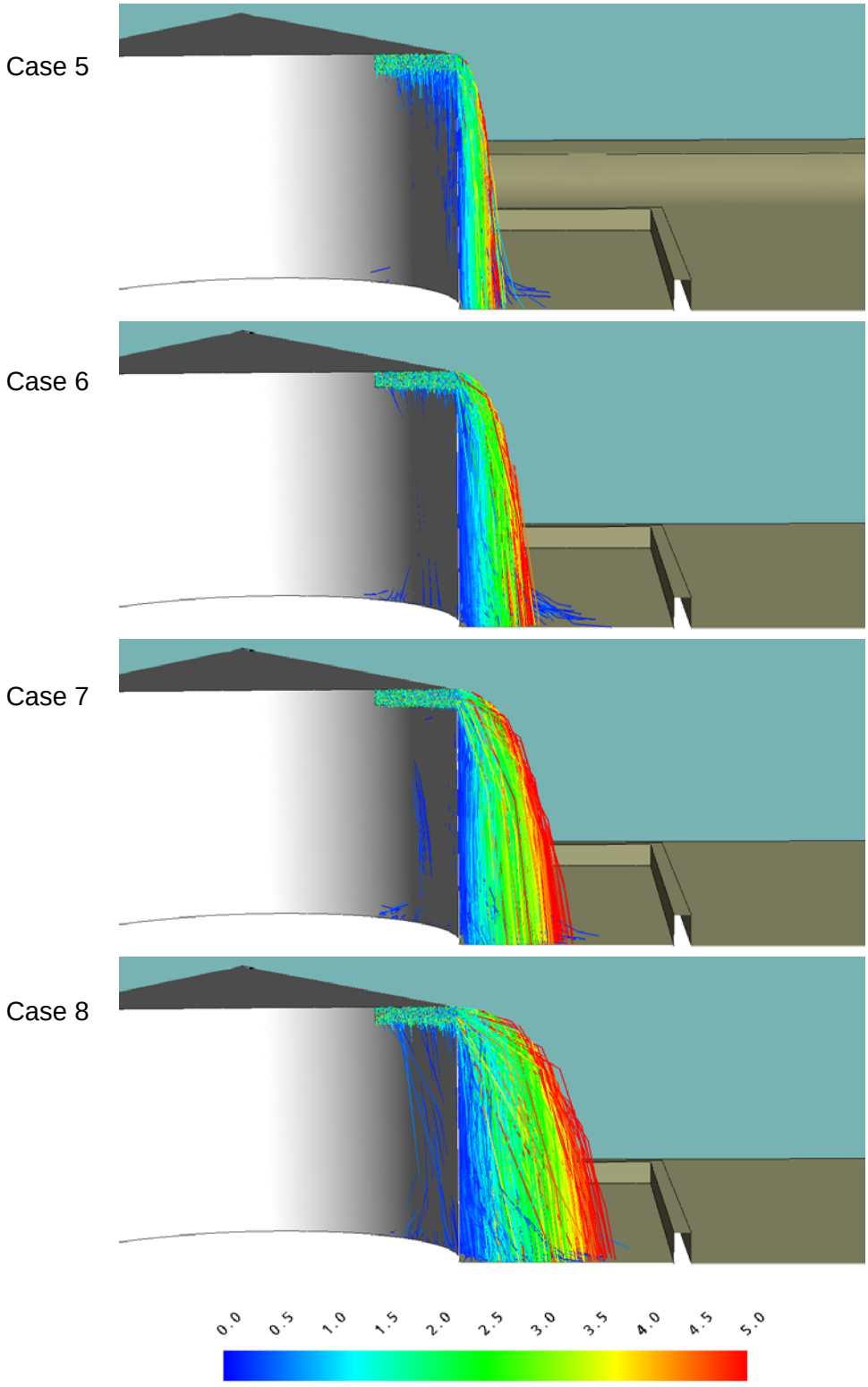

Figure 31 Cross-section through the computational domain showing the spray trajectories for Cases 5 – 8. Particle paths are coloured according to the droplet diameter using the scale shown, in millimetres. The particles appearing inside the tank walls are due to post-processing errors.

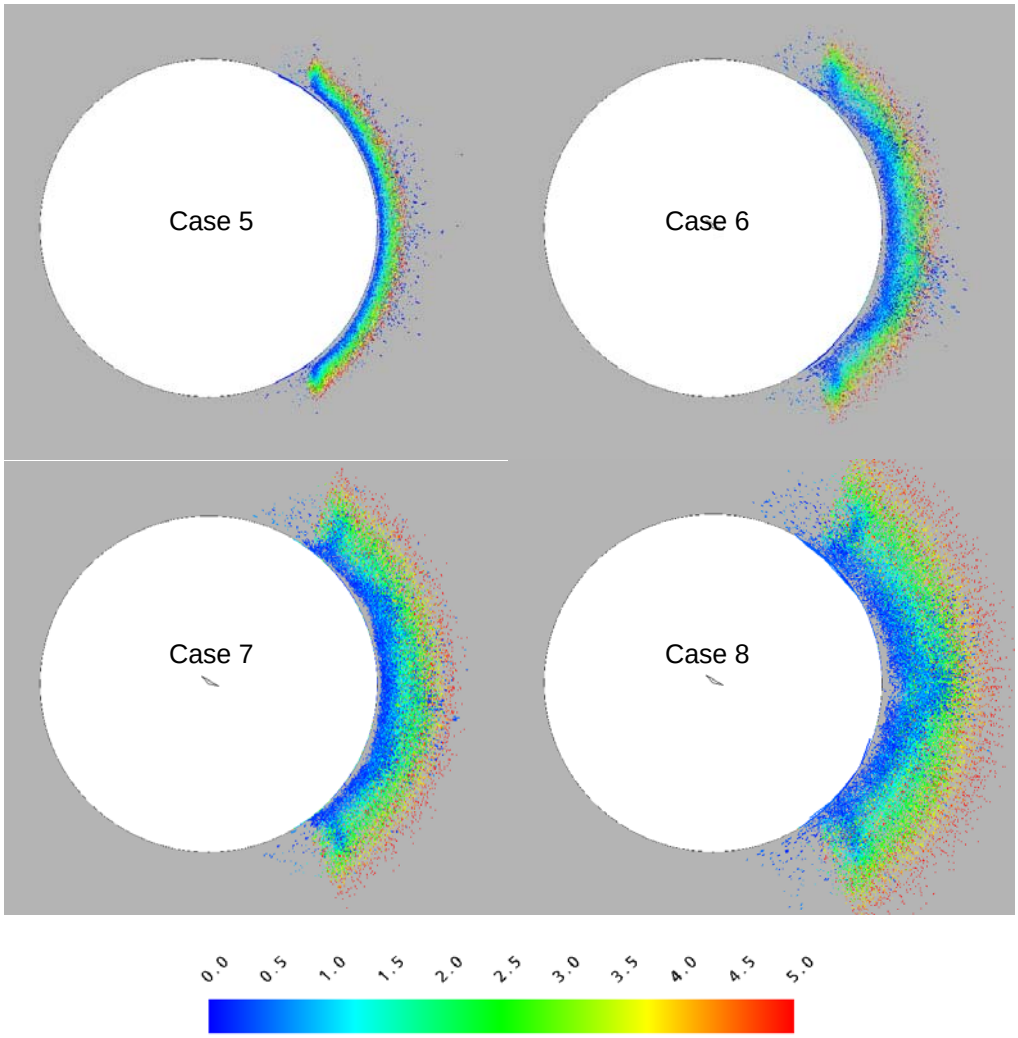

Figure 32 Distribution of spray droplets on a horizontal slice through the CFD models at a height of 1 metre above ground level for Cases 5 – 8. Droplets are coloured according to their diameter using the scale shown, in millimetres.

Figures 31 and 32 show that the smaller droplets, which are more easily convected with the air flow, fall closer to the tank wall. This is likely to be a consequence of the Coanda effect, where the air is drawn close to the tank wall. Conversely, larger droplets which have higher momentum and are less affected by aerodynamic effects fall further away from the tank.

The vapour clouds produced in Cases 5 – 8 are shown in Figures 33 and 34. Their overall shape and extent is relatively similar in each case. The cross-section view through the vapour clouds (Figure 34) shows that, contrary to the results presented in the previous Section, the vapour reaches a fully-saturated state near the tank wall and along the floor of the bund. As the spray widens so the saturated part of the vapour cloud increases in size. Interestingly, the large circular cross-section part of the vapour cloud above the bund wall is smallest for Case 8. This is probably a consequence of the spray being the most diffuse for this case, so the momentum of the vapour flowing across the floor of the bund is lower than for the other cases.

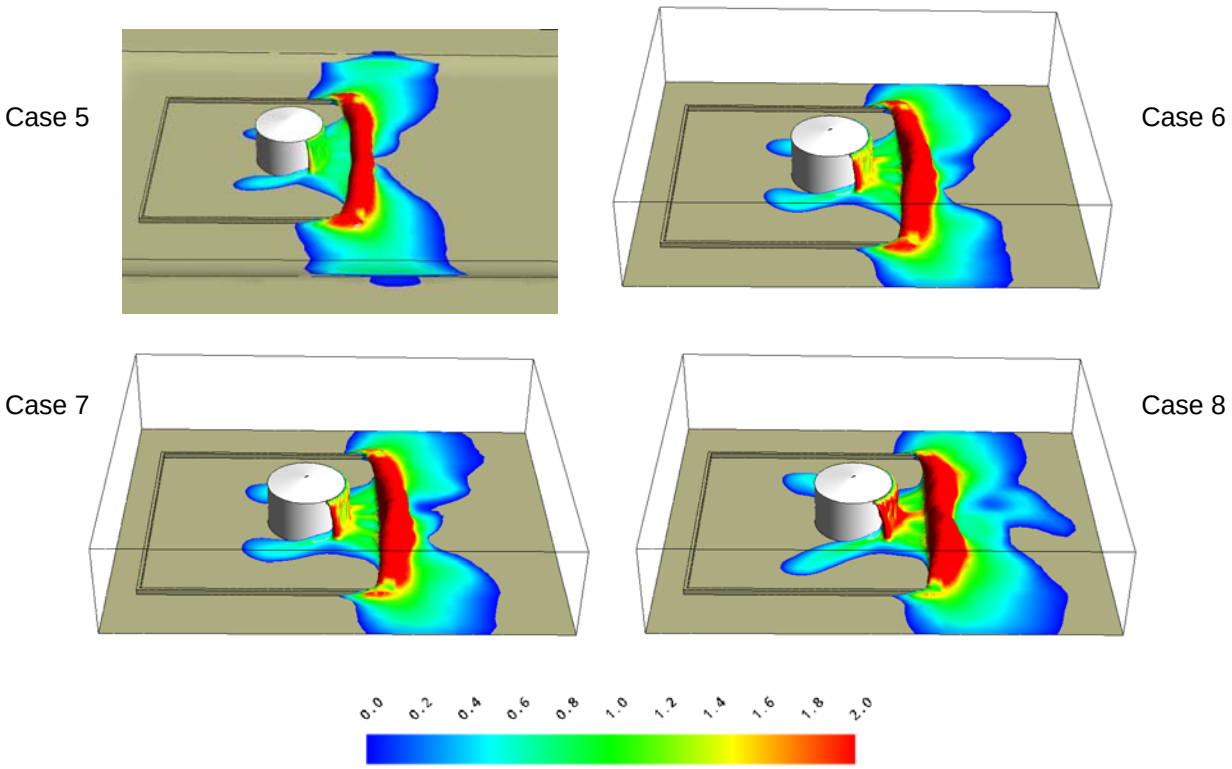

Figure 33 Visualization of the vapour cloud after 2 minutes using an iso-surface at the LEL, coloured with wall distance in metres (a similar measure to cloud depth) for Cases 5 – 8.

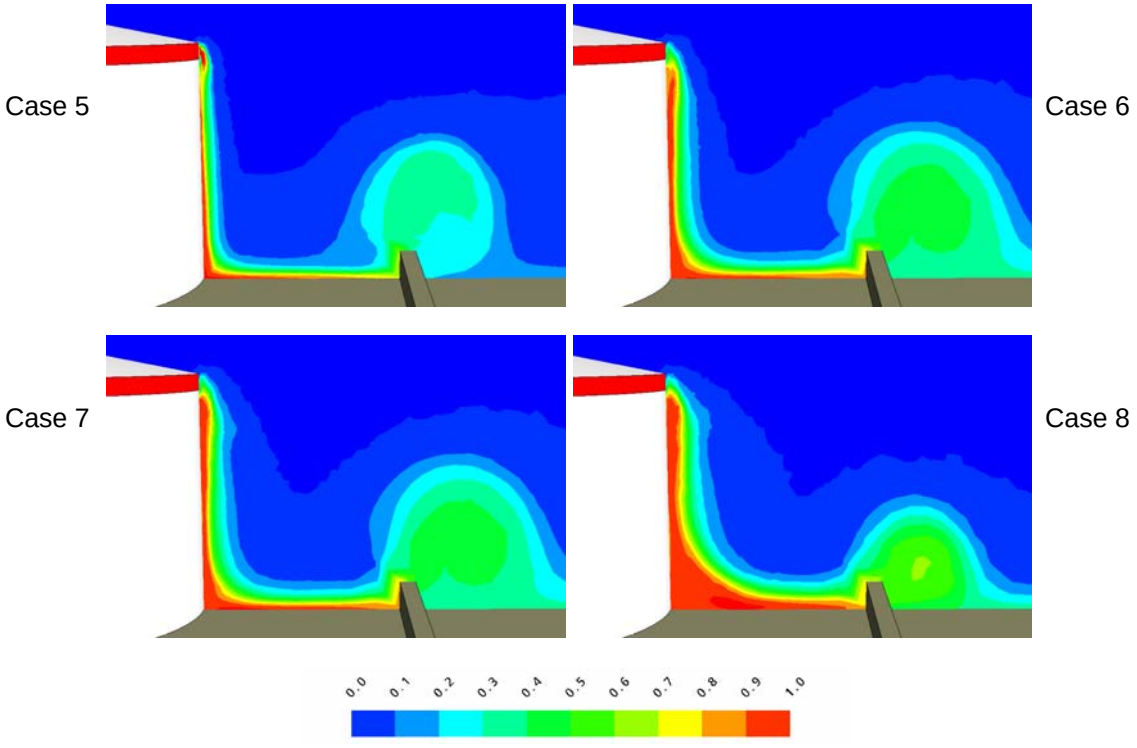

Figure 34 Contours of the ratio of the predicted vapour volume fraction to the saturation volume fraction, φ, for Cases 5 – 8.

The change in the vaporisation rate and the cloud size over time for Cases 5 – 8 are shown in Figures 35 – 37. Since a smaller domain was used in Cases 6 – 8, the vapour reached the domain boundary within the first minute and so only a relative short time interval can be analysed. The overall trends in behaviour are similar to those exhibited in Case 2, i.e. there is little or no re-entrainment of vapour back into the spray. Figure 36 shows that after 8 seconds from the start of the release the proportion of liquid vaporized reaches a constant value, indicating that fresh air is continually being drawn into the spray. For the narrowest spray (Case 5) approximately 18% of the liquid released evaporated whereas for the widest spray (Case 8) around 24% evaporated. These values are both higher than for the very narrow spray modelled in Case 2, where only around 15% of the liquid evaporated.

The size of the vapour cloud, as defined by the volume enclosed by the LEL, shows relatively little sensitivity to the spray width (Figure 37). Despite Case 8 having a spray that is three times wider than Case 5, the size of the flammable vapour cloud is only 10% larger.

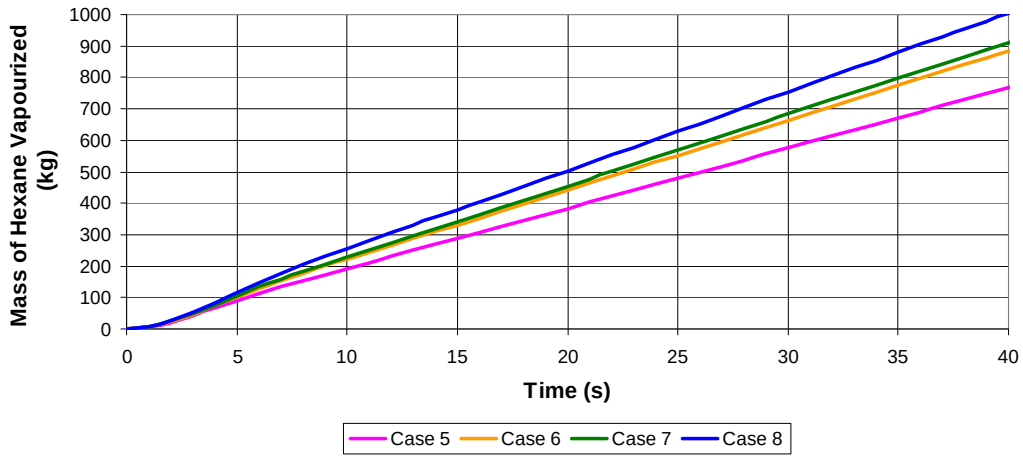

Figure 35 Predicted total mass of hexane vaporized in the spray releases as a function of time for Cases 5 – 8.

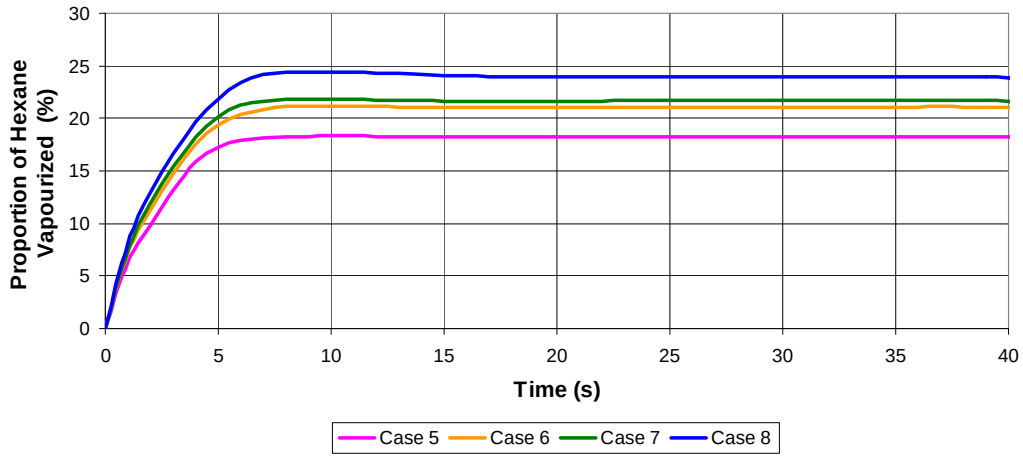

Figure 36 Percentage of hexane vaporized in the spray releases as a function of time for Cases 5 – 8.

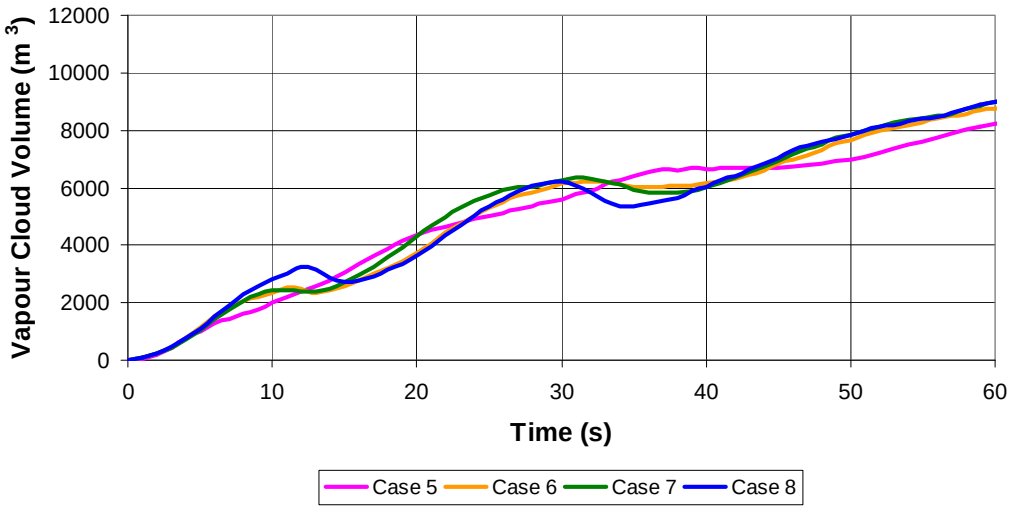

Figure 37 Growth of the vapour cloud volume over time for Cases 5 – 8. The cloud extent is defined by an iso-surface at the LEL.

4.4 SPRAY DROPLET SIZES

The CFD model predictions presented in the previous section were all made using a particular initial droplet size distribution: a Rosin-Rammler profile with characteristic diameter δ of 2.21 mm and index γ of 1.5. Most droplets were between 0 and 5 mm in diameter (Figure 33).

Experiments at HSL involving slug releases of petrol from a height of 15 metres undertaken as part of the Buncefield Investigation [1-3] found that droplets were only briefly as large as 5 mm. Within the first few metres from the point of release, droplets fragmented into smaller particles of diameter approximately 2 mm, with many droplets even smaller.

The maximum size of droplets that are aerodynamically stable is a function of the slip velocity between the fluid particle and the surrounding air, the surface tension of the fluid and other material properties. Brodkey [12] developed the following empirical correlation describing the maximum stable droplet size:

$$We = 12\left(1 + 1.077 On^{1.6}\right) \tag{6}$$

where We is the Weber number and On the Ohnesorge number[2]. The Weber number represents the ratio of disruptive hydrodynamic forces to stabilizing surface tension forces and is given by:

$$We = \frac{\rho V^2 D}{\sigma} \tag{7}$$

where ρ is the density of the fluid continuum surrounding the droplet, V the relative velocity between droplet and fluid continuum, D the droplet diameter and σ the surface tension of the droplet. The Ohnesorge number, On, characterises the viscous effects on the droplet breakup:

$$On = \frac{\mu_d}{\sqrt{\rho_d D \sigma}} \tag{8}$$

[2] *Also referred to as the Laplace number or 'Z' number.*

where μ_d and ρ_d are the dynamic viscosity and density of the droplet, respectively. The Ohnesorge number only involves droplet parameters and it implicitly assumes that the viscosity of the surrounding fluid medium is low in comparison to the droplet viscosity.

Figure 38 shows the maximum stable droplet size as a function of the slip velocity for liquid hexane droplets falling through air, based on Brodkey's correlation. This shows that for a slip velocity of 10 m/s the maximum stable droplet diameter is 2 mm. In the CFD simulations, the slip velocities reached a maximum of around 8 m/s as they neared the floor of the bund (Figure 39) which corresponds to a stable droplet diameter of around 2.5 mm.

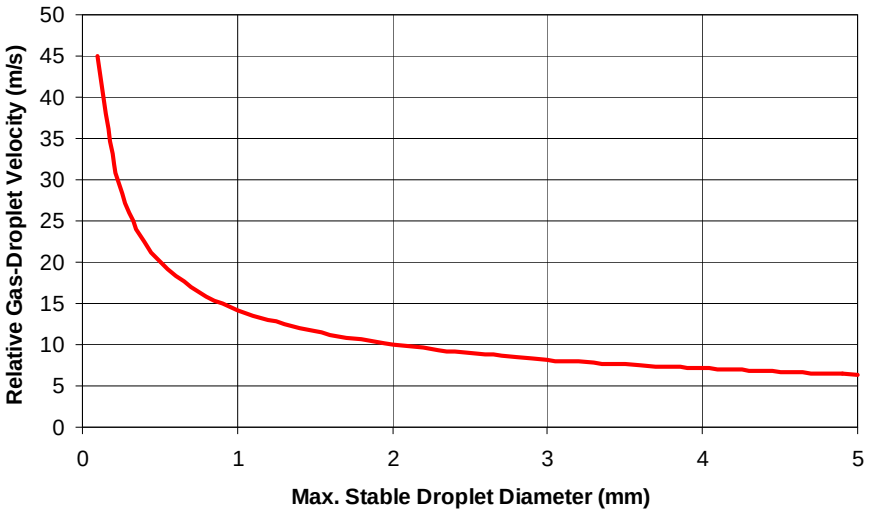

Figure 38 Maximum aerodynamically stable droplet sizes as a function of their slip velocity, from the empirical correlation of Brodkey [12].

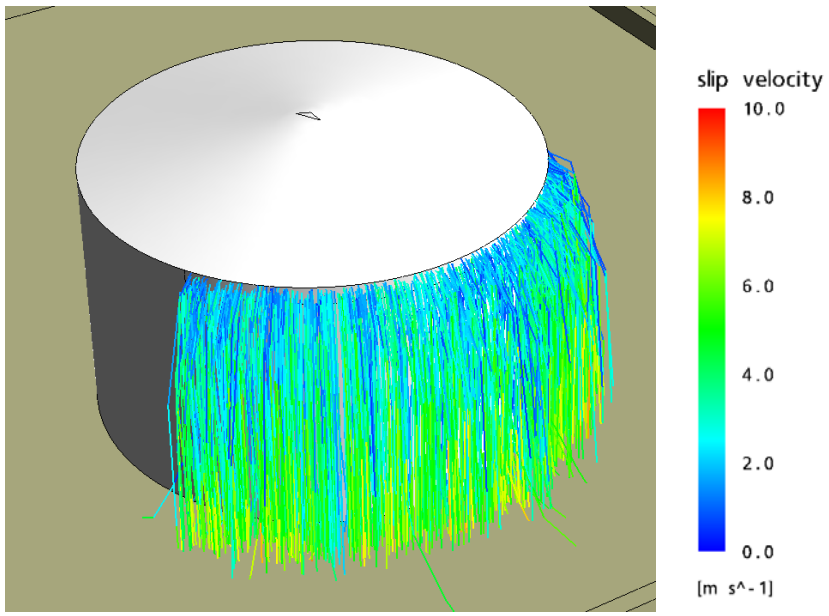

Figure 39 Droplet trajectories coloured according to the slip velocity for Case 6.

Three additional CFD simulations were undertaken to assess the sensitivity of the vapour cloud predictions to spray droplet sizes and breakup. Details of these calculations are summarized in Table 6. Cases 9 and 10 assumed initial droplet size distributions with characteristic diameters (δ) 50% lower and higher, respectively, than Case 6. The size distributions are compared in Figure 40. Case 11 used the same initial droplet size distribution as used previously in Case 6, but modelled the breakup of droplets due to aerodynamic effects. Details of the Reitz-Diwakar model [13] that was used in Case 11 can be found in Gant *et al*. [7]. The breakup model has the effect of reducing the droplet sizes as the particles fall through the air according to the local slip velocity and the droplet and vapour material properties. The droplet distributions predicted by Cases 9, 10 and 11 are compared to that obtained previously in Case 6 in Figure 41.

Table 6 Summary of the differences between Cases 6, 9, 10, 11 which examine the effect of different spray droplet sizes

Case	*Rosin-Rammler Distribution Parameters*		*Breakup Modelled?*
	δ (mm)	*γ*	
6	2.21	1.5	No
9	1.105	1.5	No
10	3.315	1.5	No
11	2.21	1.5	Yes

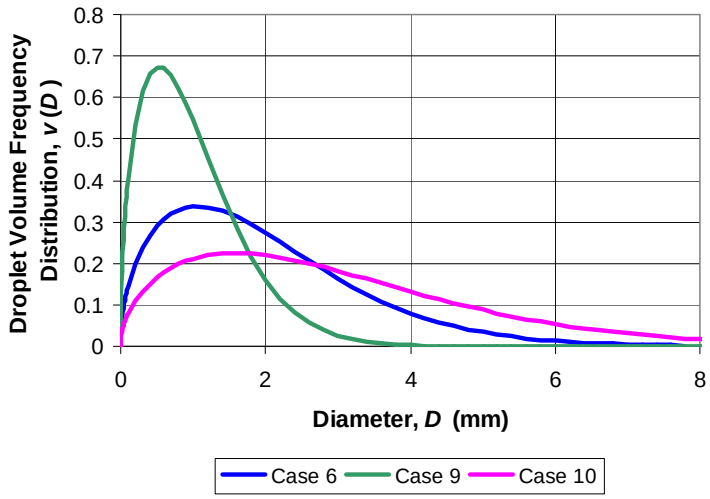

Figure 40 Rosin-Rammler droplet volume frequency distributions for Cases 6, 9 and 10.

Sprays with smaller droplets have a larger effective surface area for evaporation and consequently tend to produce larger vapour clouds. The effect is complicated since evaporation can only take place if the vapour pressure in the surrounding air is less than the equilibrium concentration. Once the air becomes saturated with vapour, no further evaporation can take place. Evaporation also causes a drop in temperature which has the effect of decreasing the equilibrium vapour pressure.

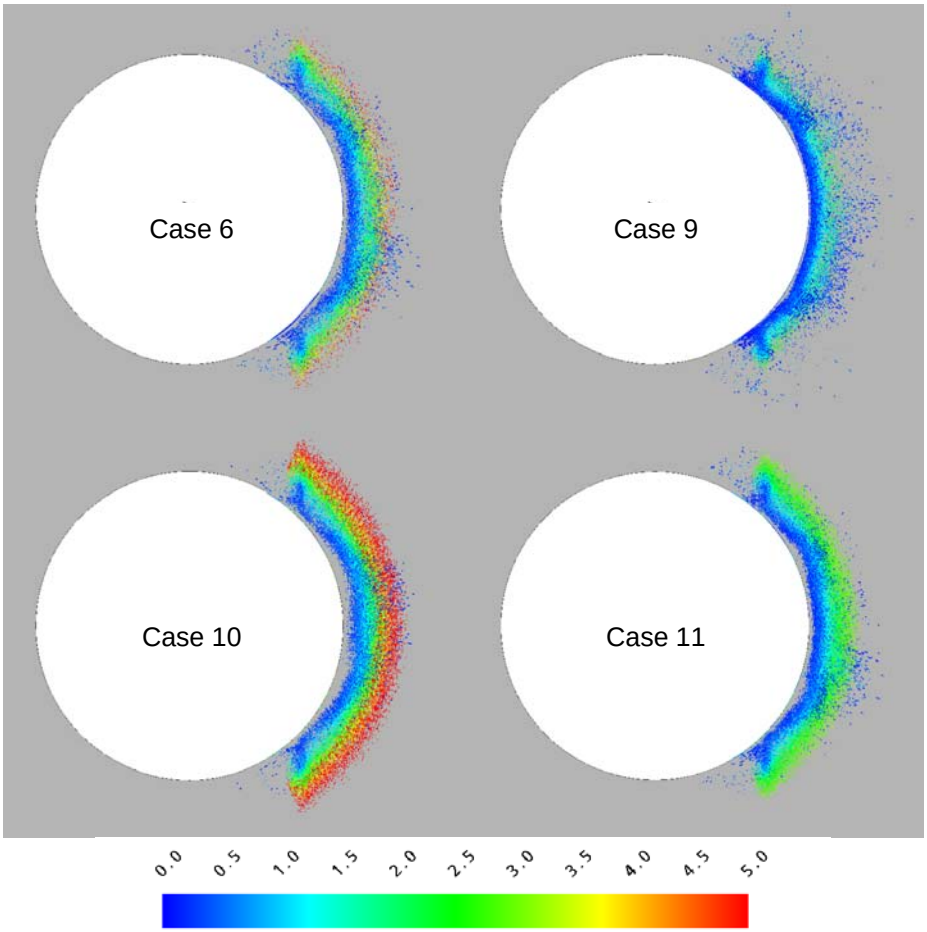

Figure 41 Distribution of spray droplets on a horizontal slice through the CFD models at a height of 1 metre above ground level for Cases 6, 9, 10 and 11. Droplets are coloured according to their diameter using the scale shown, in mm.

The ratio of the vapour concentration to the local equilibrium vapour concentration, φ, on a cross-section through the cloud is shown for Cases 6, 9 10 and 11 in Figure 42. The large droplets released in Case 10 do not evaporate sufficiently quickly to produce a fully-saturated vapour cloud. In all the other cases, the vapour clouds are saturated close to the tank wall. There are only relatively minor differences visible between Cases 6 and 9 despite there being a 50% decrease in the characteristic spray droplet size. Cases 6 and 11, with and without droplet breakup, appear practically identical to each other.

Figures 43 – 45 show the change in evaporation rate and vapour cloud size over time for the four sprays. The results with the breakup model (Case 11) again appear almost identical to those of Case 6 without a breakup model. This is likely to be a consequence of the evaporation rate being mainly controlled by the smaller droplets, which evaporate more readily. Since the same initial droplet size distribution was used in Cases 6 and 11 and only the larger droplets breakup, the quantities of small (sub 2 mm) droplets was similar in Cases 6 and 11.

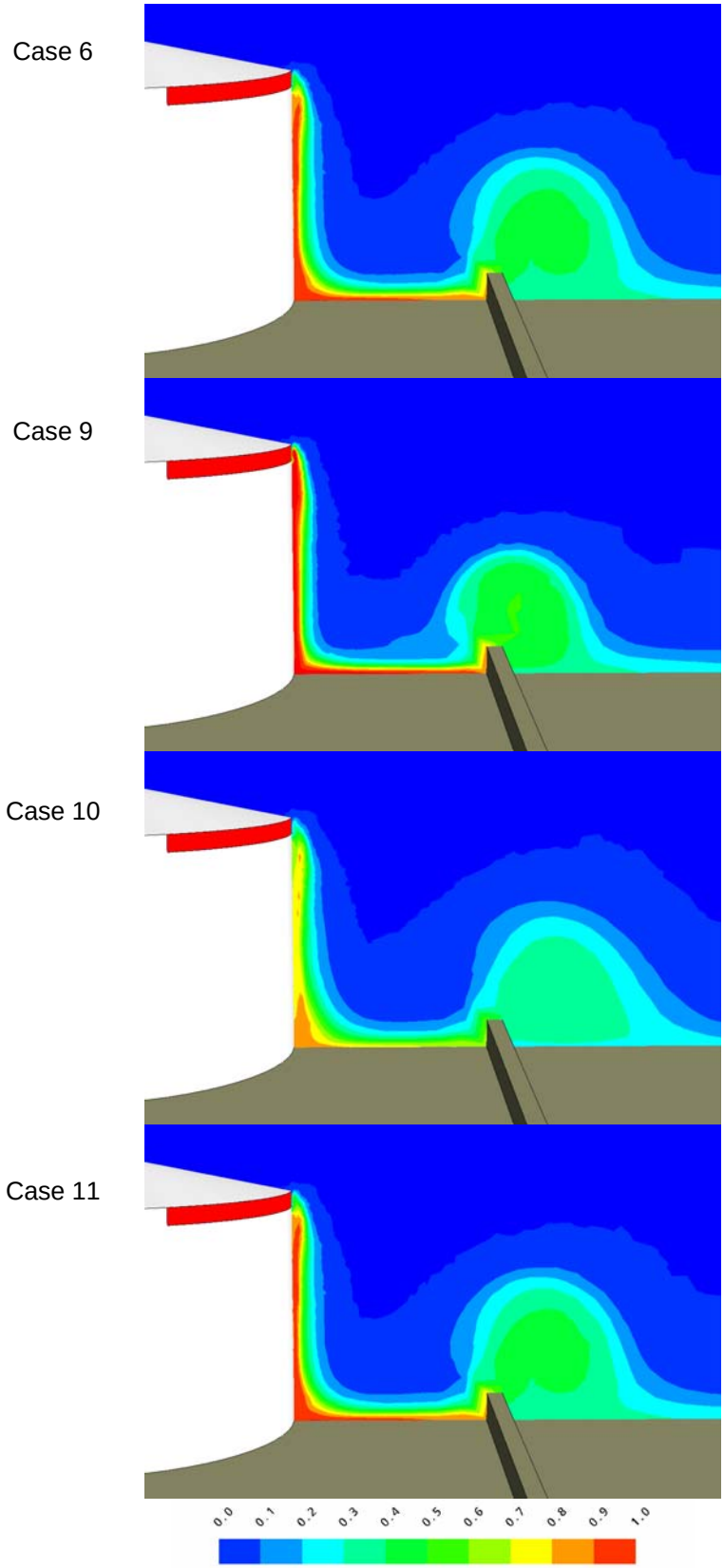

Figure 42 Contours of the ratio of the predicted vapour volume fraction to the saturation volume fraction, φ, for Cases 6, 9, 10 and 11.

When the droplets released were small (Case 9), approximately 23% of the liquid released evaporated into the air whereas when larger droplets were released (Case 10), only 18% of the liquid evaporated (Figure 44).

The flammable cloud generated by the spray with small droplets (Case 9) was 40% larger than that generated by the larger droplets (Case 10) after one minute (Figure 45). Clearly the droplet size is an important factor in controlling the size of the vapour cloud.

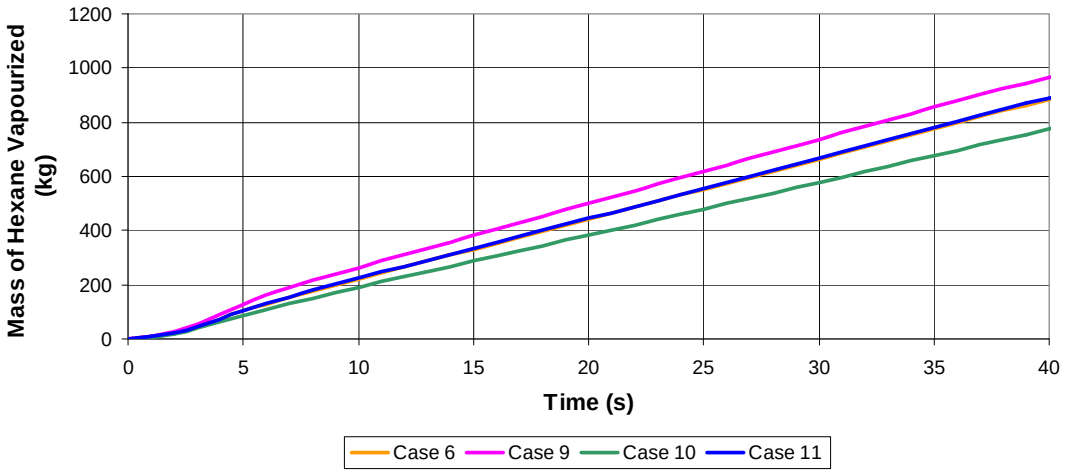

Figure 43 Predicted total mass of hexane vaporized in the spray releases as a function of time for Cases 6, 9, 10 and 11.

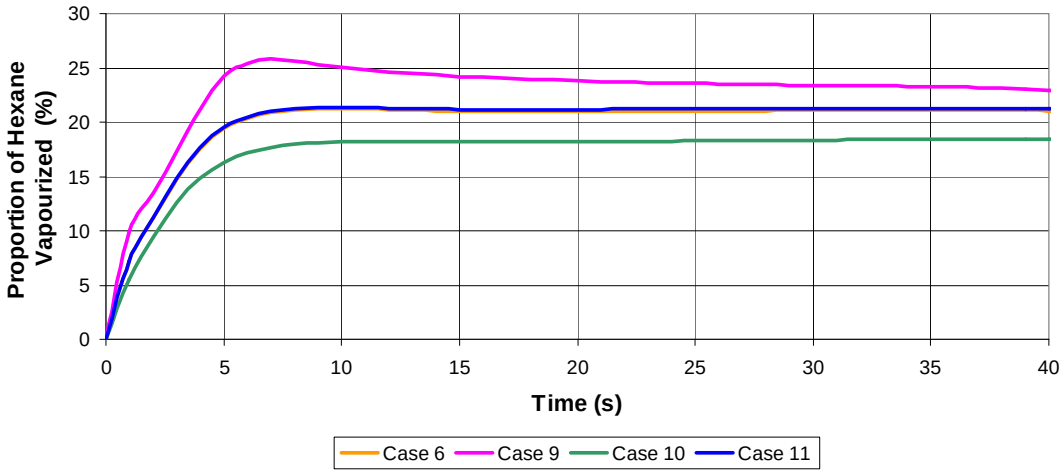

Figure 44 Percentage of hexane vaporized in the spray releases as a function of time for Cases 6, 9, 10 and 11.

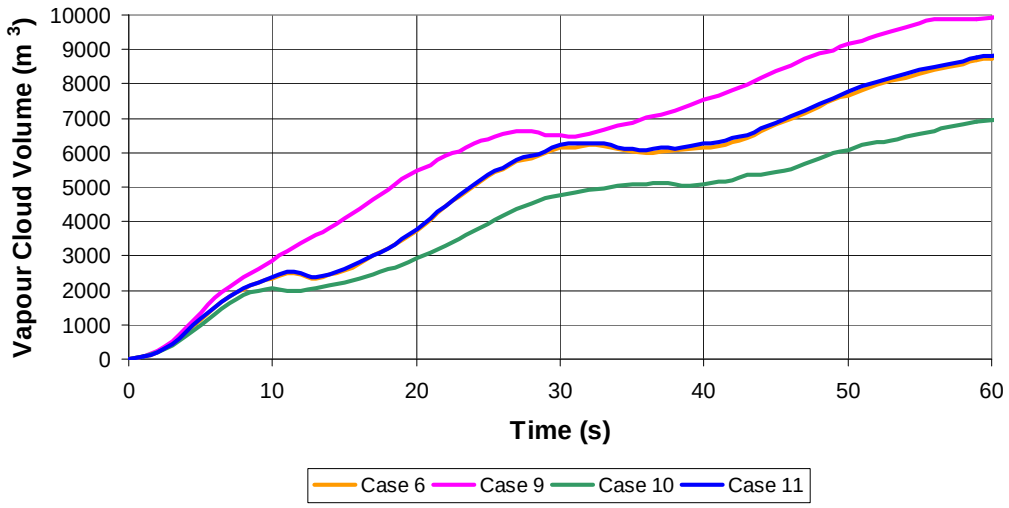

Figure 45 Growth of the vapour cloud volume over time for Cases 6, 9, 10 and 11. The cloud extent is defined by an iso-surface at the LEL.

4.5 SPRAY DISTRIBUTION AROUND THE TANK PERIMETER

As discussed earlier, there are three main designs of crude-oil/petroleum-product storage tanks in the UK: floating deck tanks, fixed roof tanks with vents and fixed roof tanks with pressure/vacuum valves. The spray release behaviour from each of these tanks in an overfilling scenario is likely to be different. All of the previous simulations have concentrated on a single release from one-third of the tank rim. Such a model is intended to represent a release from a floating-deck tank where the overspill occurs from one side of the tank (perhaps because the floating deck is stuck at an angle or the top rim of the tank is not at a uniform level). To help explore how sensitive the CFD model results are to other types of release mechanism, two further calculations were made:

- **Case 12**: a release from eight orifices, each of 15˚ width, evenly distributed around the tank rim. This model simulates a fixed roof tank with multiple vents, similar to the Buncefield release.

- **Case 13**: a single 360˚ release, evenly distributed around the tank rim to simulate a floating deck tank with no fixed roof, spilling evenly around the full tank perimeter.

Three-dimensional views of these models and the geometry used previously are shown in Figure 46.

Another possible release scenario that could be considered is from a fixed roof tank fitted with a pressure/vacuum valve. However, it is thought that this would be likely to lead to a narrow, very dense spray from a small split in the rim of the tank. The quantity of vapour produced by such a spray is likely to be much smaller than for Cases 12 and 13 due to the limited air entrainment that would take place. This scenario has therefore not been modelled.

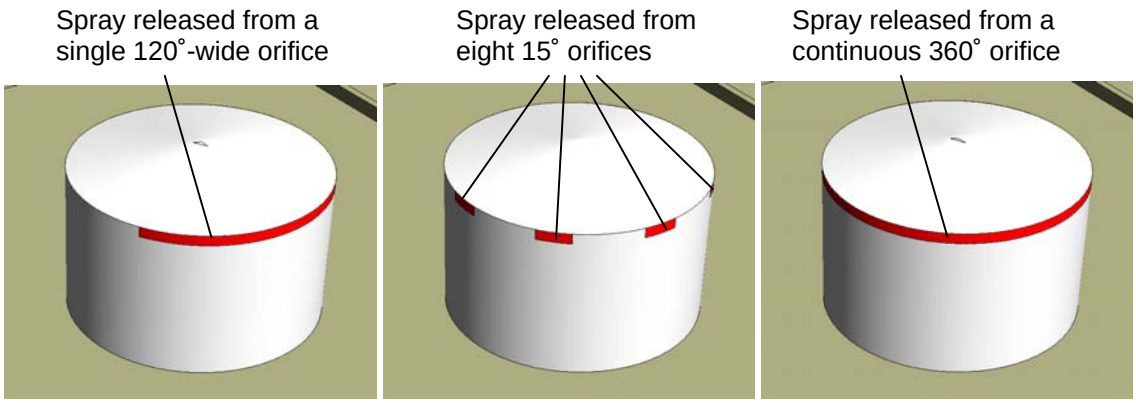

Figure 46 Three-dimensional views of the storage tanks showing the orifices (in red) from where spray droplets are released in Cases 6, 12 and 13.

In order to compare to the earlier results, Cases 12 and 13 used the same spray conditions as those of Case 6. A summary of these conditions are given again below:

- Hexane droplets are released with an initial diameter given by the Rosin-Rammler size distribution (δ = 2.21 mm and γ = 1.5) at a temperature of 15 ˚C.
- Droplet breakup is ignored.
- Total liquid mass flow rate is 105 kg/s.
- Tank dimensions are: diameter 25 m, height 15 m, 1:5 pitched roof.
- Ambient conditions: zero wind speed, temperature 0 ˚C.

In Cases 6, 12 and 13, the spray droplets are released in the CFD model from 1-metre-high orifices around the upper rim of the tank, shown in red in Figure 46. The total orifice area is identical in Cases 6 and 12, since the eight 15˚-wide orifices in Case 12 have identical area to the single 120˚-wide orifice in Case 6. Therefore Cases 6 and 12 share the same initial spray mass density (4.0 kg/s/m^2). The orifice area for Case 13 is three times larger, since it wraps around all 360˚, so the initial spray mass density is 1.3 kg/s/m^2.

The flammable vapour clouds produced by Cases 6, 12 and 13 after two minutes are shown in Figure 47. The clouds are clearly of very different shape; in Case 12 the eight separate sprays impinge onto the floor of the bund producing an alternating pattern of peaks and troughs in the vapour cloud around the base of the tank. For Case 13, where the release takes place around the whole perimeter of the tank, the vapour cloud produced in the floor of the bund is more uniform.

Despite the significant differences in cloud shape between Cases 6 and 9, the amount of vapour produced is practically identical (Figure 48). In both cases, approximately 21% of the liquid is vaporized (Figure 49). This indicates that the distribution of the spray has relatively little effect on the amount of vapour produced, provided that the spray mass density is unchanged. The volume of the flammable vapour cloud in Case 12 is generally less than that from Case 6, by up to 35% at times (Figure 50). This appears to be a consequence of the interaction of the vapour cloud with the bund wall and different air entrainment rates associated with the different shapes of the vapour cloud.

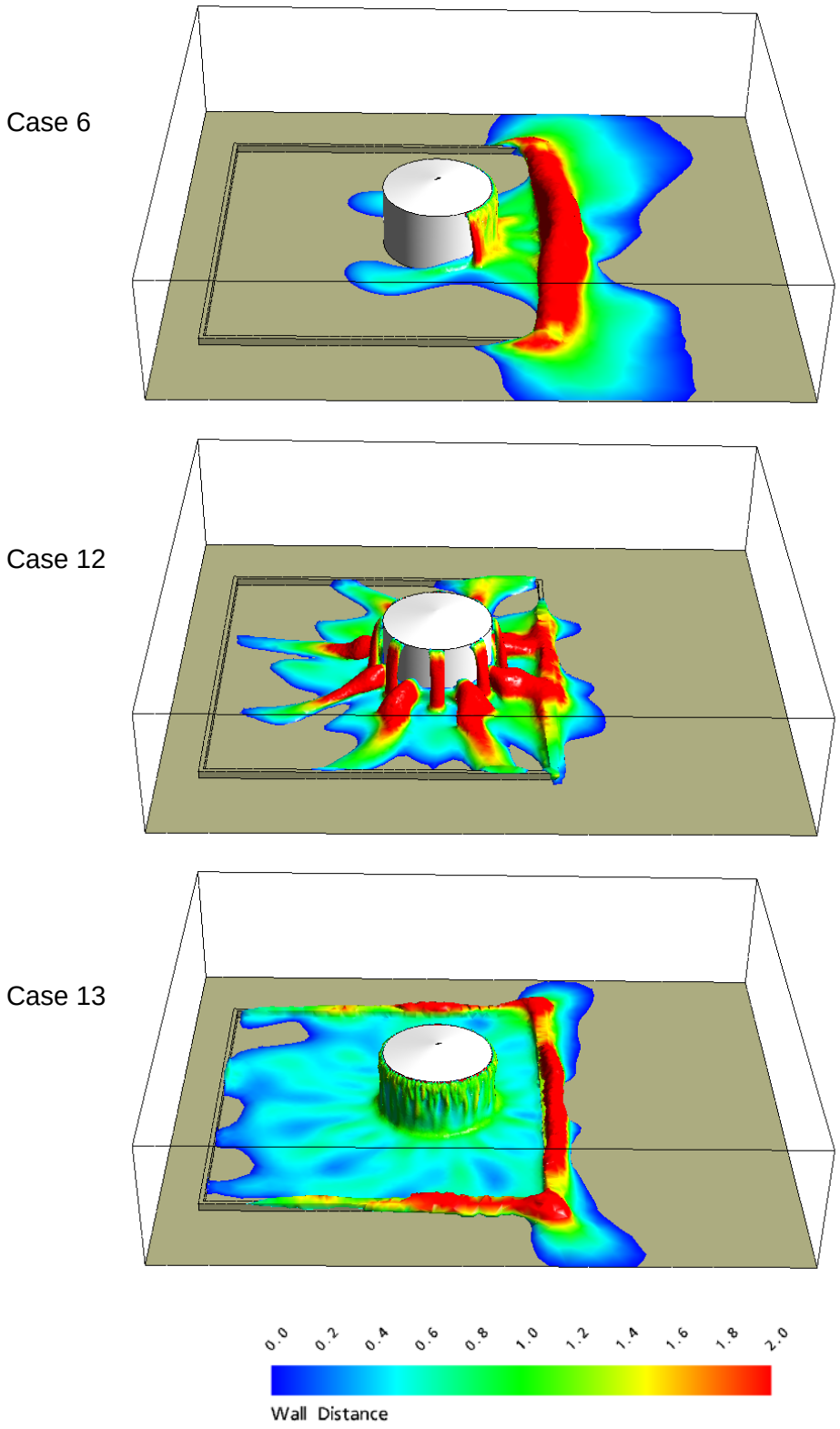

Figure 47 Visualization of the vapour cloud using an iso-surface at the LEL, coloured with wall distance in metres (a similar measure to cloud depth) after 2 minutes from the start of the release for Cases 6, 12 and 13.

The amount of vapour produced in Case 13, where the spray is uniformly distributed around the perimeter of the tank, is significantly higher than either Case 6 or 12. Approximately 28% of the liquid released is vaporized (nearly one-third higher than for Cases 6 or 12). This is a consequence of the spray mass density being three times lower in Case 13, i.e. the amount of air that is entrained into the spray is proportionally much higher for Case 13 than for Cases 6 or 12.

Although more vapour is produced in Case 13, it does not produce a significantly larger flammable cloud than Cases 6 or 12. The trends are complicated to generalise as the cloud volumes do not increase linearly over time; for the first 40 seconds of the release the cloud is larger in Case 13 but from then until 1 minute it is smaller than in Case 6. The flammable cloud volumes time-averaged over the first minute of the release for Cases 6, 12 and 13 are 5122, 4361 and 5182 m^3 respectively. The flammable cloud produced by Case 13 is therefore marginally larger than the other two cases on average.

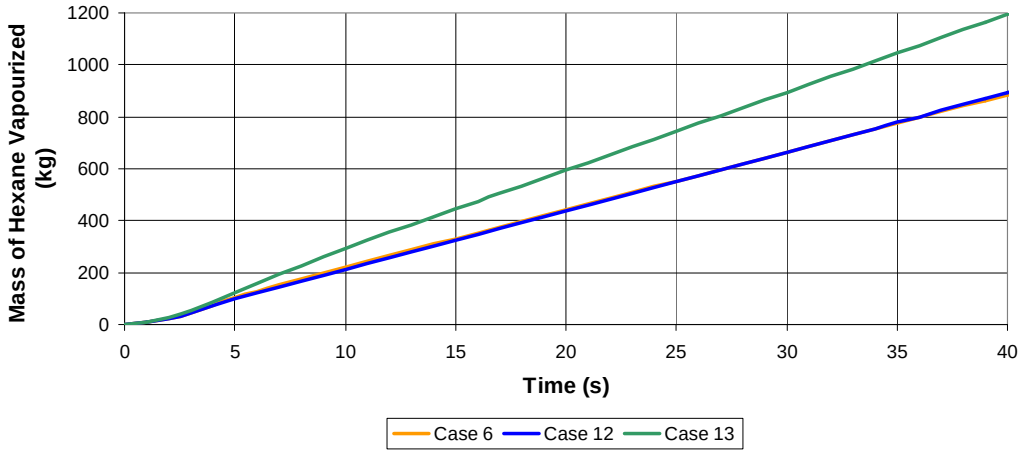

Figure 48 Predicted total mass of hexane vaporized in the spray releases as a function of time for Cases 6, 12 and 13.

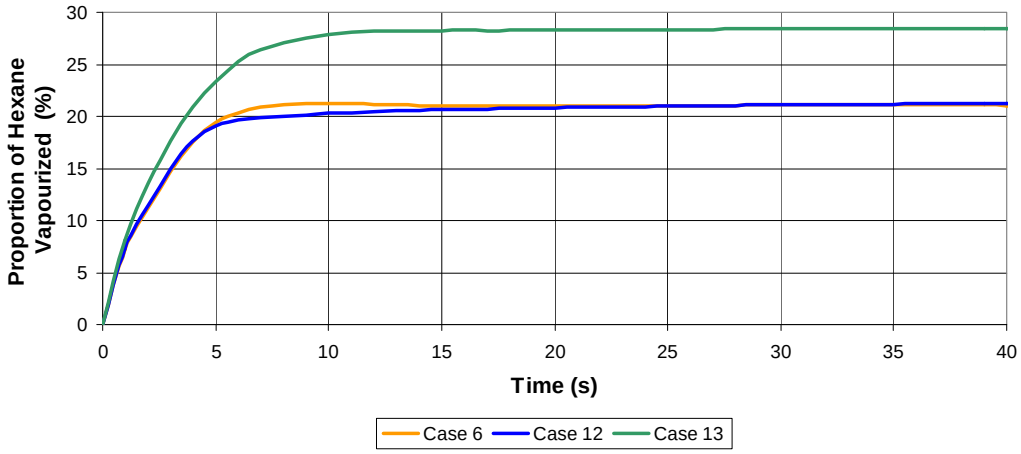

Figure 49 Percentage of hexane vaporized in the spray releases as a function of time for Cases 6, 12 and 13.

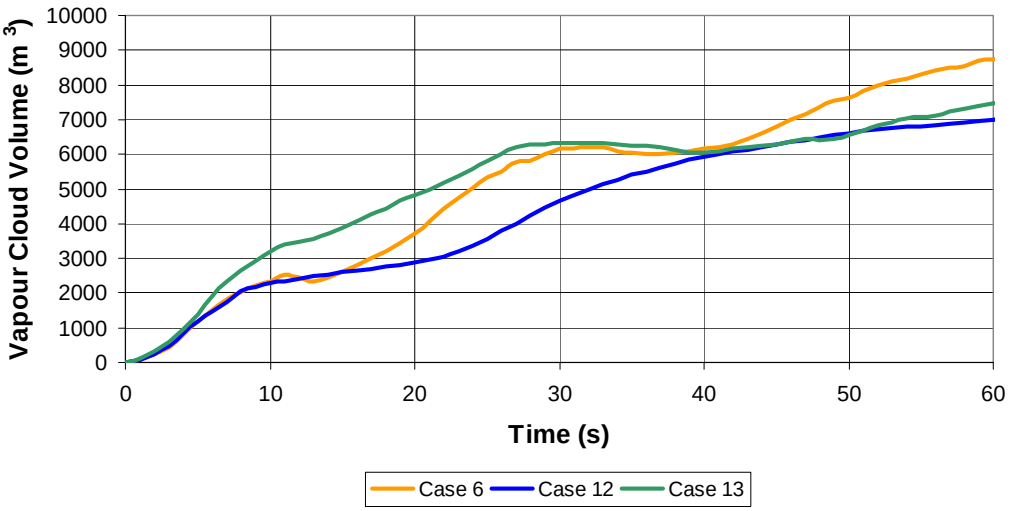

Figure 50 Growth of the vapour cloud volume over time for Cases 6, 12 and 13. The cloud extent is defined by an iso-surface at the LEL.

4.6 OBSTACLES OUTSIDE THE BUND

In the Buncefield Incident, the dispersion of flammable vapour appeared to be strongly influenced by the presence of obstacles close to the overfilling tank and other local topological effects (e.g. elevated ground levels). To investigate whether obstacles outside the bund might have a significant impact on the amount of liquid vaporized, an additional CFD simulation was undertaken in which the bund was surrounded by a 5-metre-high porous hedge. Details of hedge porosities can be found in the agricultural engineering literature, for example Bean *et al*. [14]. For the present calculations, the porosity of the hedge was assumed to be 40%, the same as the dense hedges modelled in the Buncefield Incident.

In order to enable comparisons to be made to the earlier results, the spray release conditions from Case 6 have been used. The extent of the flammable vapour cloud two minutes after the start of the release is shown in Figure 51. The porous hedge, shown in green in the Figure, clearly has a significant affect on the dispersion of the cloud; the vapour builds up behind the hedge before filtering through it and dispersing across the ground. The cross-section through the vapour cloud (Figure 52) shows that the vapour reaches a considerable height between the bund wall and the hedge. However, there does not appear to be any re-entrainment of vapour from the cloud back into the spray region and fresh air is continually drawn into the spray from above. This can be seen more clearly in the streamlines presented in Figure 53.

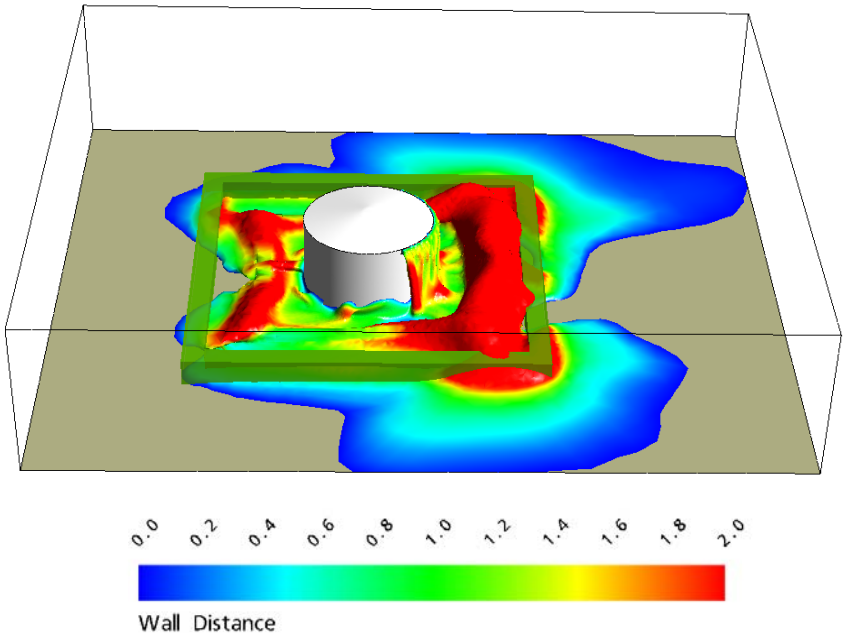

Figure 51 Visualization of the vapour cloud in Case 14 after 2 minutes using an iso-surface at the LEL, coloured with wall distance in metres (a similar measure to cloud depth).

Since there is no re-entrainment of vapour into the spray, the amount of vaporization is similar to that found previously in Case 6 (Figures 54 and 55). However, Figure 56 shows that the volume of vapour in the flammable range reaches significantly higher values as the vapour builds up behind the hedge. One minute after the release, the flammable vapour cloud is 35% larger with the hedge (Case 14) than without (Case 6).

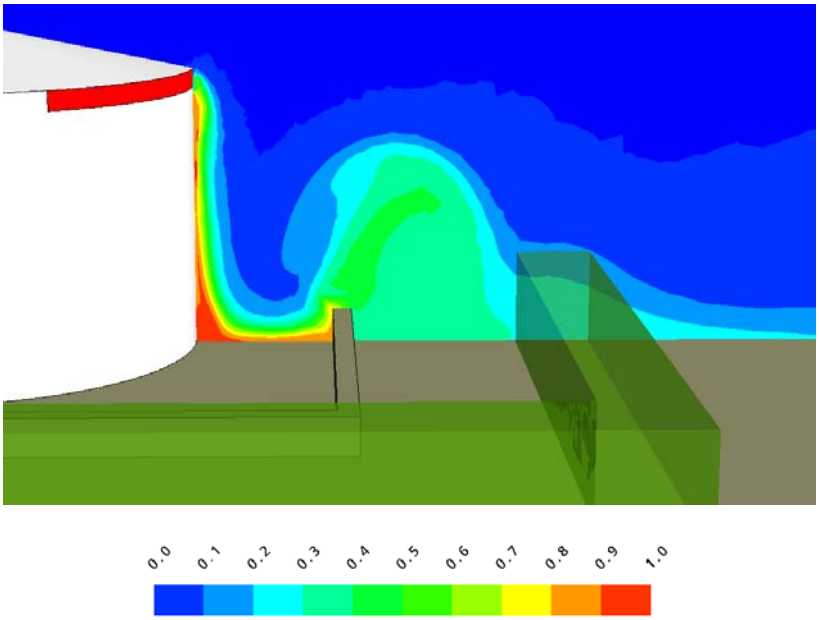

Figure 52 Contours of the ratio of the predicted vapour volume fraction to the saturation volume fraction, φ, for Case 14 after two minutes.

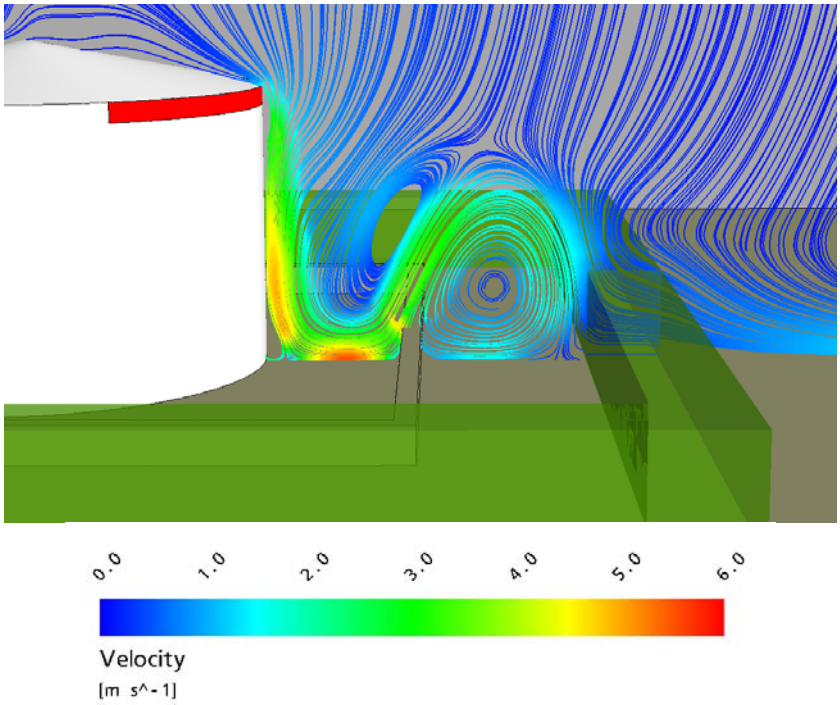

Figure 53 Streamlines coloured with the velocity magnitude for Case 14 after two minutes.

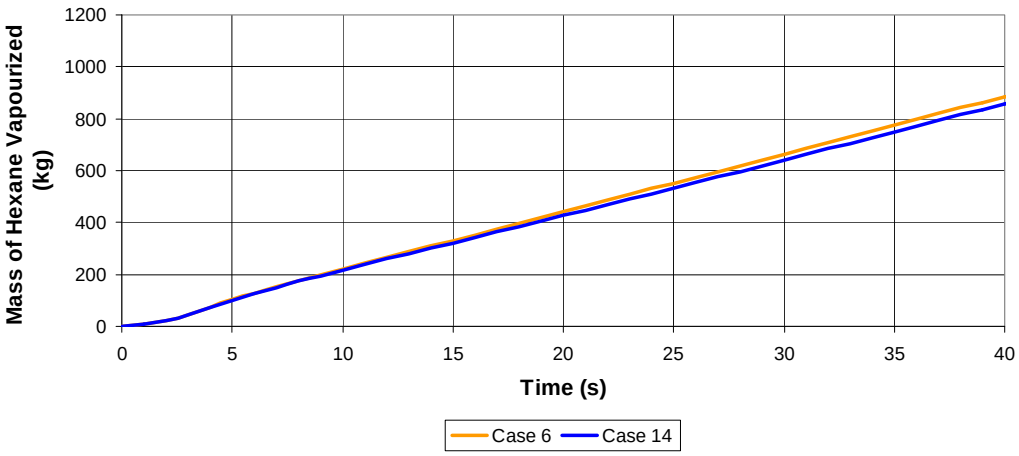

Figure 54 Predicted total mass of hexane vaporized in the spray releases as a function of time for Cases 6 and 14.

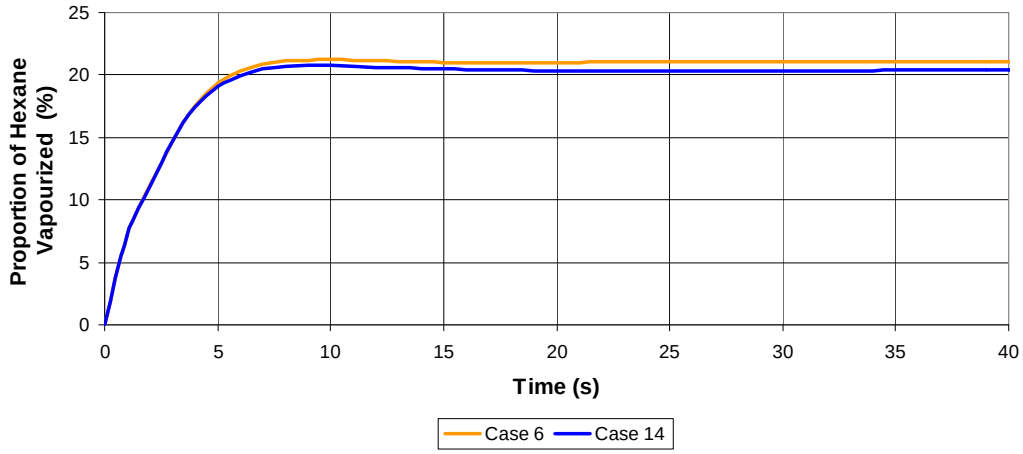

Figure 55 Percentage of hexane vaporized in the spray releases as a function of time for Cases 6 and 14.

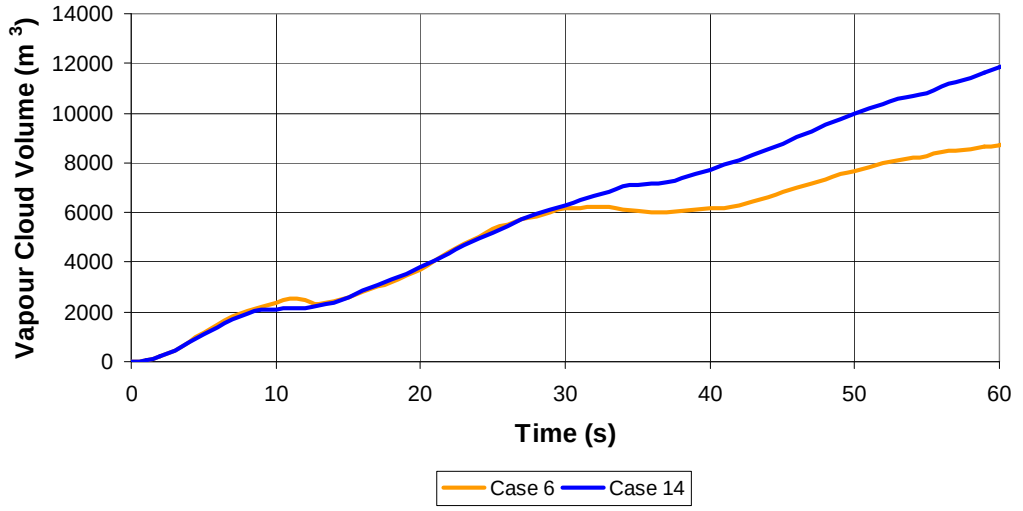

Figure 56 Growth of the vapour cloud volume over time for Cases 6 and 14. The cloud extent is defined by an iso-surface at the LEL.

4.7 MODELLING EVAPORATION FROM A LIQUID POOL

In the tank release calculations documented in the previous sections, evaporation from the liquid pool formed around the overfilling tank has been ignored. Only evaporation from the spray of droplets has been modelled. Initially, in the early stages of this study, the evaporation from the pool was considered to be of secondary importance compared to that from the spray of droplets, since they have a larger surface area for evaporation.

Estimating the amount of evaporation from the liquid pool in an overfilling incident is challenging due to the non-uniform flow of air and vapour over the liquid surface. The flow near the tank is similar to an impinging jet hitting the liquid surface at right-angles, whilst further away from the tank the air/vapour flows parallel to the liquid surface. The evaporation rates are likely to be different in these two flow regions, with possibly higher evaporation in the

impinging-jet region. The CFD software, CFX[3], used in the present study does not yet have the capability to model pool evaporation.

HSE uses a pool evaporation model for risk analysis called GASP, produced by ESR Technology[4] [15, 16]. The model assumes a constant flow of air parallel to the liquid surface. Tests have been undertaken using GASP to predict the evaporation rate from a pool of hexane. These have been based on the following conditions:

- Liquid release rate: 84 kg/s
- Discharge velocity: 5 m/s
- Discharge Temperature: 15˚C
- Ambient Temperature: 0˚C
- Bund diameter: 71.5 m

The release rate of 84 kg/s is based on the total mass release rate of the liquid in the previous spray analyses (105 kg/s) assuming that 20% of the mass evaporates in the spray prior to it forming the pool. The bund radius and ambient temperature are based on the Buncefield Incident conditions.

Figure 57 shows the vaporization rate two minutes after the start of the release as a function of the wind speed predicted using GASP. The results show clearly that as the wind speed increases so the evaporation rate increases; a doubling in the wind speed from 4 to 8 m/s leads to an increase in vaporization rate from 2 to 3.5 kg/s. In the spray release scenarios modelled previously using CFD (Sections 4.2 – 4.6), the vapour velocity varied between 0 and 6 m/s close to the floor of the bund.

The variation in the predicted vaporization rate over time using the GASP model with a fixed wind speed of 5 m/s is shown in Figure 58. The vaporization rate increases linearly until the liquid spill fills the entire floor area of the bund, after which time the vaporization rate remains constant. For this wind speed, the vaporization rate reaches a maximum of just over 4 kg/s, equivalent to around 4% of the total amount of liquid released from the tank. This compares to the CFD simulations that predicted vaporization rates of between 14% and 28% from the spray (Sections 4.2 – 4.6).

Further tests with the GASP model (not presented here) showed that the results were relatively insensitive to the discharge velocity in the range 1 – 10 m/s.

[3] http://www.ansys.com/products/cfx.asp
[4] http://www.esrtechnology.com

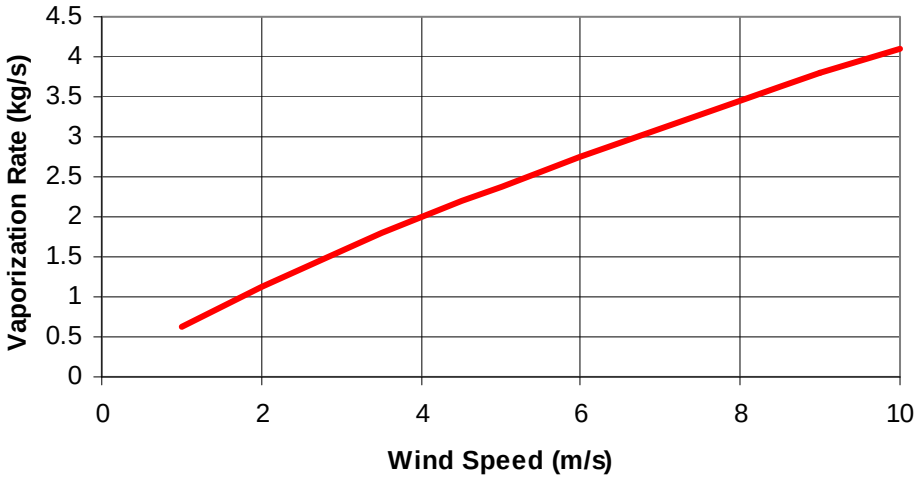

Figure 57 Pool vaporization rate as a function of wind speed predicted using GASP two minutes after the start of the release.

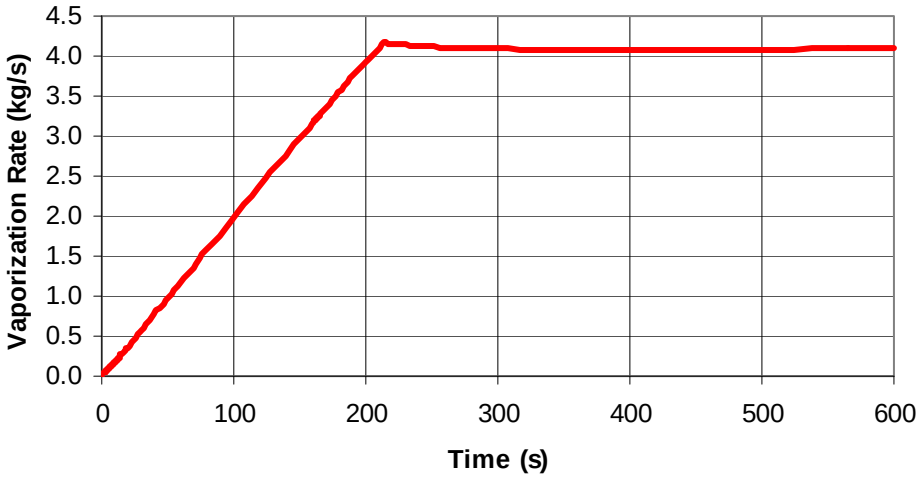

Figure 58 Evolution of the pool vaporization rate over time predicted using GASP with a constant wind speed of 5 m/s.

The analysis using GASP suggests that pool evaporation could account for one quarter to one eighth of the total amount of vapour produced. However, it should be emphasised that the evaporation model used in GASP assumes a constant flow of fresh air parallel to the surface of the pool. This differs in two ways from the flow pattern produced in a tank-overfilling incident. Firstly, in a in a tank overfilling incident the air close to the tank impinges nearly at right angles onto the pool surface. This would be likely to lead to enhanced pool evaporation. Secondly, the air passing over the pool will already contain some hexane/petrol vapour, due to evaporation from droplets in the liquid cascade, and not pure fresh air as assumed by GASP. This will produce lower pool evaporation rates compared to those predicted by GASP.

In principle, it is possible to configure CFD models to simulate a pool of liquid evaporating around an overfilling tank (modelling both impinging-jet and parallel-flow regions and accounting for the modified concentration gradients). One example of how the evaporation process might be modelled is described in the recent paper by van Limpt *et al*. [17]. To implement this approach in a commercial CFD code would require additional user-defined Fortran subroutines to interface with the CFD code.

Another approach that could be adopted to model pool evaporation is to use the well-documented analogies between evaporation, or mass transfer, and heat transfer [18, 19]. These analogies consist of simple equations relating the Sherwood number, *Sc* (a mass transfer coefficient), to the Nusselt number, *Nu* (a heat transfer coefficient). Using these relations, the heat and mass transfer relations for a particular geometry would be interchangeable. If the amount of heat transfer from a heated flat surface was known, it would be possible to infer the amount of evaporation from a liquid pool of the same surface shape. CFD models have been used extensively to predict the amount of heat transfer from heated surfaces (e.g. [20-22]). It would therefore seem possible to model pool evaporation by replacing the floor of the bund with a heated surface. The heat transfer rates calculated by the CFD model for this case could then be transformed into an equivalent mass transfer rate. There would still be some uncertainty in using the heat/mass transfer analogies in the impingement region of the flow where the boundary-layer approximations underlying the heat/mass transfer analogies are not applicable. Evidence of the breakdown of momentum/heat analogies in impingement zones is documented in Chung *et al*. [23], although Angioletti *et al*. [24] provide a counter-example of where the heat/mass transfer analogy is applied in an impinging flow. This approach has the advantage of not requiring additional user-coded CFD subroutines but would involve greater uncertainty.

4.8 SUMMARY

In Sections 4.2 – 4.6, the consequences of changing a number of different parameters on the production of vapour in a tank overfilling incident was examined. To help understand the relative importance of the different factors, Figures 59 and 60 show the variance in the vaporization rate, R, and mean flammable cloud volume, $\overline{V}$.

The method used to calculate the variance of the vaporization rate (Figure 59) is best explained in terms of an example. In Cases 5 – 8 the effect of the spray width on the vapour production rate was examined. After 30 seconds from the start of the release, for Cases 5, 6, 7 and 8 the percentage of liquid vaporized was 18.3%, 21.1%, 21.7% and 23.9% respectively. The difference between the highest and lowest vaporization rates was: 23.9 – 18.3 = 5.6%. As a proportion of the mean vaporization rate the variance is:

$$variance = \frac{5.6}{(23.9 + 18.3)/2} = 26.5\% \qquad (9)$$

The variance in the predicted vaporization rate for the other cases was calculated similarly.

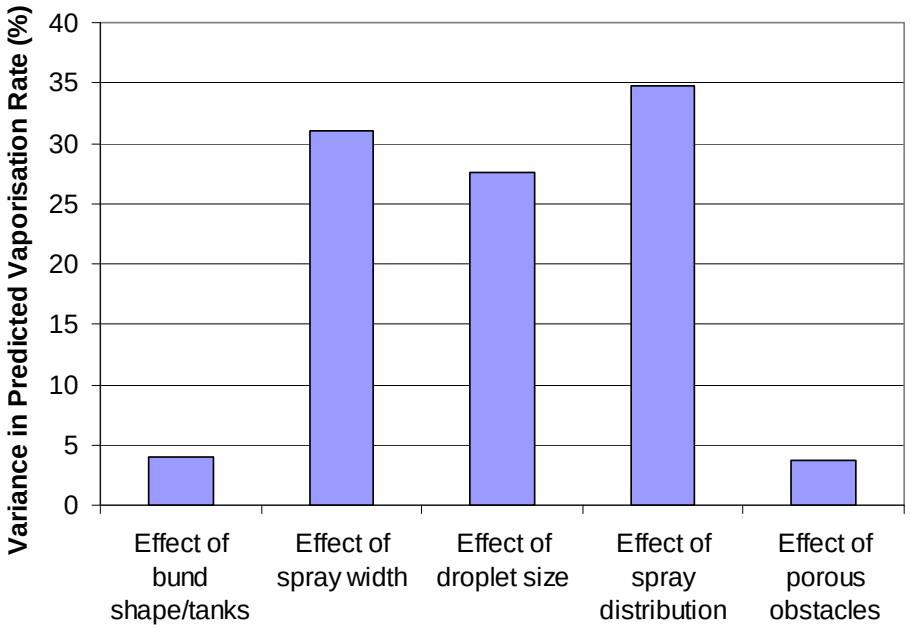

Figure 59 Variances of various factors on the predicted vaporisation rate.

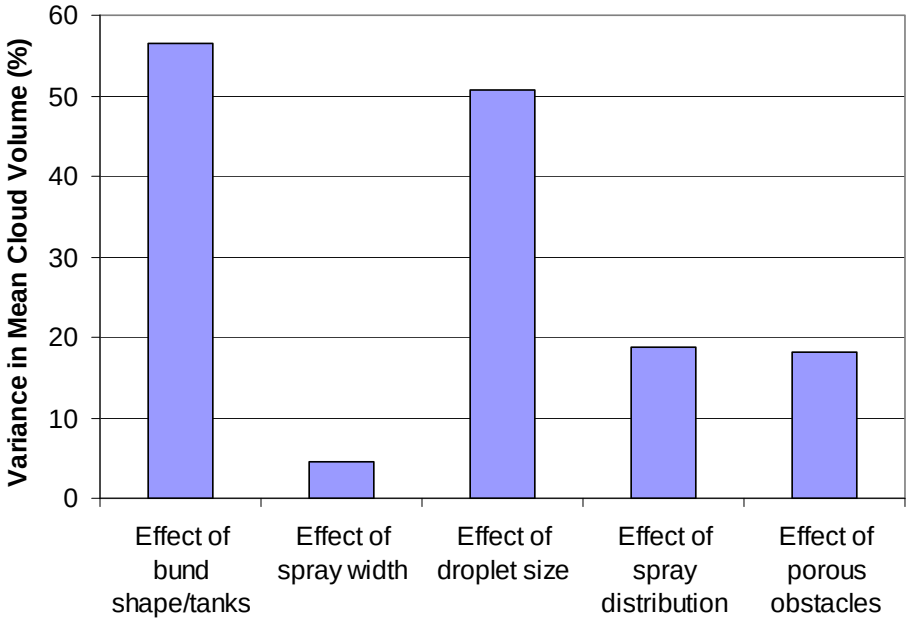

Figure 60 Variances of various factors on the predicted vapour cloud volume averaged over the first minute of the release.

In all of the different scenarios modelled, the proportion of liquid vaporized reached a practically constant value soon after the release started. In contrast, the flammable cloud volume did not reach a constant value for the duration of the CFD simulations in most cases (Figures 25, 37 and 45). Consequently, the variance in cloud volume after 20 seconds is different to that after 40 seconds. Rather than select arbitrarily an instant in time to calculate the variances, the time-averaged flammable cloud volume over the first minute of the release has been used.

The time average of the flammable cloud volume, $\overline{V}$, is calculated from:

$$\overline{V} = \frac{1}{T}\int_0^T V(t)dt \approx \frac{1}{T}\sum_0^T V(t).\Delta t \tag{10}$$

where $V(t)$ is the vapour cloud volume at time and the integral period T is 60 seconds. In most cases, the cloud volume was recorded every second and so the time interval Δt used was 1 second.

The variances shown in Figures 59 and 60 provide an indication of the relative importance of various factors in determining the vaporization rate and the flammable cloud volume. The vaporization rate appears to be affected by three main factors: the droplet size, the width of the spray and the distribution of the liquid around the tank perimeter. The second and third factors relate to the spray mass density in that spreading the same mass of liquid over a larger area, i.e. decreasing the spray mass density, causes the amount of vaporization to increase. It was shown earlier that if the spray mass density was kept constant but the distribution pattern changed, the vaporization rate remained the same. The effect of any obstacles around the tank on the vaporization rate appears to be minimal.

Figure 60 shows that there are two main factors affecting the size of the vapour cloud: the shape of the bund/presence of other tanks and the spray droplet size. The spray distribution and the presence of other obstacles around the tank also have a secondary effect whereas the spray width appears to have little influence on the vapour cloud volume.

It might be reasonable to expect that the main factors which control the amount of vapour production will also be most important in affecting the size of the vapour cloud. Figures 59 and 60 show that this is generally not the case. The amount of flammable vapour is affected strongly by air entrainment and dilution. Although two different types of spray release might produce the same vaporisation rate, if one is released much more energetically than the other and entrains more fresh air into the vapour cloud, the volume of the two flammable clouds will be different.

An example of this phenomenon is given by the results presented in Section 4.3, where the width of the spray was varied. This appears to have a relatively minor effect on the flammable cloud volume whereas it has a strong affect on the vaporization rate. Figure 34 shows that as the width of the spray increases, the amount of vapour within the bund increases but the size of the recirculation zone just downstream of the bund wall decreases. This is due to the mass density of the spray falling into the bund decreasing as the spray width increases: rather than producing a dense, high-velocity spray it is more dispersed. This in turn produces a lower velocity vapour flow so that when it impacts into the bund wall the flow recirculation immediately downstream of the bund wall becomes smaller, producing a smaller overall cloud volume. The two effects appear to be competing against each other: a less dense spray produces more vapour within the bund but a smaller recirculation downstream. If the bund wall was taken away, the flow behaviour might be very different and the spray width might appear to be a more significant factor.

The sensitivity of the vaporisation rate and cloud size to the various factors is likely to be inter-dependent, i.e. changing both droplet size and spray distribution at the same time will probably produce different behaviour than that implied by modelling their respective effects independently. In the analysis presented here only one parameter has been varied at a time. A more thorough understanding of the flow behaviour might be gained by varying multiple factors at the same time.

One potentially important aspect of the flow that has not been considered in the CFD modelling presented here is the phenomenon of droplet splashing. The simulations in this report treat the droplets as "disappearing" upon contact with the floor. In reality, some fraction of the liquid will become re-suspended in the air following its impact with the wetted surface of the bund floor. Droplet splashing is likely to have two effects. Firstly, it will increase the aerodynamic drag on the flow of vapour across the bund floor; the rebounding splash products will be carried away in the vapour flow and the transfer of momentum from the vapour to the droplets will reduce the speed of the vapour. Secondly, the presence of fine droplets in the vapour flow may increase the concentration of the vapour leaving the bund. Further work is necessary to assess the importance of these effects.

Droplet splashing is a complex physical phenomenon and the characteristics of the splash products depends on the size of incident droplets, their velocity and material properties, the shape and characteristics of the impingement surface and whether it is dry, wetted or a deep pool. It should be possible to simulate splashing in a CFD model by injecting droplets with a prescribed velocity vertically upwards from the floor of the bund, within the splash zone. However, the parameters to input into such a model are largely unknown. Although some data on droplet splashing exists in the scientific literature, most of this is related to flows inside internal combustion engines. To select the appropriate velocity, size and mass flux of rebounded droplets for a tank-overfilling incident requires experiments to be performed using a configuration as close as possible to the real-life situation.

5 DISCUSSION & CONCLUSIONS

This report documents ongoing research aimed at understanding the important factors affecting the production of flammable vapour in incidents where large storage tanks of volatile liquids are overfilled. The work provides a first step towards developing a model which will predict the likely size of flammable vapour clouds based on simple measures such as the tank dimensions, tank design type, pumping rates and liquid composition.

Three main types of storage tank have been identified which are each likely to produce different flow behaviour in the event of overfilling: fixed roof tanks with vents, fixed roof tanks with pressure/vacuum valves and floating deck tanks with no fixed roof. The likely release scenarios from overfilling releases for each of the tank designs has been discussed.

CFD simulations have shown that the vaporisation rate in a tank-overfilling incident is mainly affected by the size of the spray droplets, the distribution of the spray around the circumference of the tank and the width of the spray. A fine spray of droplets over a large area will lead to the highest vapour production rates.

The spray distribution and spray width both control the spray mass density, i.e. the mass of spray droplets per unit volume. If liquid is released around the full 360˚ perimeter of a tank then, for a given pumping rate, the mass density of the spray will probably be lower than if all of the liquid is released from a single small orifice. Also, if the spray is produced very energetically, for instance by impingement of the liquid onto the tank's wind-girder at high speed, a disperse spray will be produced with low mass density. A lower spray mass density provides more fresh air in contact with the droplets and hence higher evaporation rates. If the spray is sufficiently dispersed and composed of sufficiently small droplets that the core of the vapour flow becomes completely saturated, no further evaporation can take place in this region. This implies that a model of the vapour production rate should be based on the shape of the spray as well as its mass density and the size of the droplets.

The initial size of spray droplets is affected by the primary breakup mechanism that fragments the continuous stream of liquid flowing out of the tank into discrete droplets, for example due to impingement of the liquid stream onto the deflector plate around the rim of a tank. The droplets produced by this primary breakup mechanism then free-fall from the tank and are subject to secondary breakup due to aerodynamic instability, turbulence and collisions between droplets. The maximum stable size of these falling droplets is a function of the slip velocity between the droplets and the air, and the liquid's material properties (surface tension, density and viscosity).

Predicting the primary breakup of liquid streams into discrete fragments is difficult and subject to significant uncertainty. The approach taken in the current study has been to ignore primary breakup and instead assign the droplets an initial size distribution. The proportion of small droplets in this initial size distribution has been shown to affect significantly the vapour production rate. It is recommended that further detailed experiments be undertaken to help quantify the likely size distribution of droplets produced in tank overfilling releases.

The size of the flammable cloud produced in a tank overfilling release appears to be not solely a function of the vaporisation rate and there are other important factors that need to be considered. In particular, CFD simulations have shown that the design and location of the bund wall and the presence of obstacles around the tank affect the size of the flammable cloud. This suggests that a simple model for predicting the size of vapour clouds will need to take account of the location of the tank and its surroundings as well as the tank dimensions, pumping rate, liquid composition etc. This brings additional and undesirable complexity into the model. One option

would be to base a universal model on a 'worst case' scenario. In the preliminary CFD analysis presented in this report, a vertical bund wall next to the tank was found to produce the largest flammable cloud. The distance from the bund wall to the tank was shown to affect the size of the cloud and this requires further study to identify the appropriate worst case situation.

The ambient conditions (wind speed, temperature, atmospheric stability) will also strongly affect the dispersion of the cloud but in the present study only an assumed worst case scenario similar to conditions present during the Buncefield Incident have been modelled.

All of the CFD simulations undertaken in this work have ignored vapour produced by pool evaporation. Initially, this was thought to be justified on the basis that the surface area of the pool was small compared to the total surface area of all the droplets in the spray. However, tests using the pool-evaporation model, GASP, and further consideration of the likely mass transfer rates close to the tank, where the flow is similar to an impinging jet, justify further investigation. Two possible approaches to simulate pool evaporation using CFD models have been outlined. One requires additional functionality to be added to the CFD code and another makes use of heat/mass transfer analogies and involves simulating a heated plate instead of a liquid pool. It is recommended that both alternatives are investigated. To provide confidence in the accuracy of the techniques, a short validation study should be undertaken comparing the two models performance against GASP and experimental data in a simple pool evaporation scenario.

Future work should also consider modelling the splashing of droplets as they hit the floor of the bund. In the CFD simulations presented in this report, the droplets "disappear" on contact with the floor. Splashing is likely to have two effects: a reduction in the speed of the vapour flowing across the bund and an increase in the vapour concentration.

The sensitivity of the various factors investigated in this report has been explored using a parametric approach, i.e. changing only one parameter at a time whilst keeping all others constant. A more thorough understanding of the flow behaviour would be gained by varying multiple factors at the same time since it is likely that, for example, the droplet size and spray mass density may be inter-dependent in how they affect the vapour production rate. The simulations presented here are also preliminary in the sense that numerical errors have not been assessed by performing a grid and droplet-count dependence study. The sensitivity of model results to the choice of turbulence treatment has also not been examined.

It is clear from the above discussion that the development of a well-validated simple model for the prediction of flammable clouds from tank overfilling incidents will require fairly substantial further investigation. The recommended program of work involves both experimental and numerical simulations of realistic releases, with challenges for both measurement and mathematical modelling. Whilst a conservative approach could be adopted to help reduce the necessary effort (e.g. assuming a fine spray of droplets with a low mass density) an overly-conservative model could predict the formation of hazardous flammable clouds in release scenarios which in reality would not produce significant quantities of vapour.

6 REFERENCES

1. *Buncefield Investigation Progress Report*, Major Incident Investigation Board (MIIB) (available from http://www.buncefieldinvestigation.gov.uk) 21 February, 2006.

2. *Buncefield Investigation Second Progress Report*, Major Incident Investigation Board (MIIB) (available from http://www.buncefieldinvestigation.gov.uk) 11 April, 2006.

3. *Buncefield Investigation Third Progress Report*, Major Incident Investigation Board (MIIB) (available from http://www.buncefieldinvestigation.gov.uk) 9 May, 2006.

4. Maremonti, M., G. Russo, E. Slazano, and V. Tufano, *Post-accident analysis of vapour cloud explosions in fuel storage areas.* Trans. IChemE, **77**, p360-365, 1999.

5. Yuill, J. *A discussion on losses in process industries and lessons learned*. in 51st Canadian Chemical Engineering Conference (see http://psm.chemeng.ca), Halifax, Nova Scotia, Canada, 2001.

6. Persson, H. and A. Lönnermark, *Tank Fires: Review of fire incidents 1951 - 2003*, SP Report 2004:14, SP Swedish National Testing and Research Institute, 2004.

7. Gant, S.E., A.J. Heather, and A. Kelsey, *CFD modelling of evaporating hydrocarbon sprays*, HSL Report CM/07/04, 2007.

8. Harris, R.E., *The Investigation and Control of Gas Explosions in Buildings and Heating Plant*, E & F N Spon Ltd, London, in association with the British Gas Corporation, 1983.

9. Yoon, S.S., J.C. Hewson, P.E. DesJardin, D.J. Glaze, A.R. Black, and R.R. Skaggs, *Numerical modeling and experimental measurements of a high speed solid-cone water spray for use in fire suppression applications.* Int. J. Multiphase Flow, **30**(11), p1369-1388, 2004.

10. Walmsley, S.J., *A computational and experimental study of the sprays produced by fire suppression sprinkler systems*, PhD Thesis, Mech. Eng. Dept., University of Manchester Institute Science & Technology (UMIST), Manchester, UK, 2000.

11. Chow, W.K., *Application of computational fluid dynamics in building services engineering.* Building & Environment, **31**(5), p425-436, 1996.

12. Brodkey, R.S., *The Phenomena of Fluid Motions*, Addission-Wesley, Reading, Mass., USA, 1969.

13. Reitz, R.D. and R. Diwakar, *Effect of drop breakup on fuel sprays*, SAE Technical Paper Series, No. 860469, 1986.

14. Bean, A., R.W. Alperi, and C.A. Federer, *A method for characterizing shelterbelt porosity.* Agricultural Meteorology, **14**, p417-429, 1975.

15. Webber, D.M. and S.J. Jones. *A Model of Spreading Vaporising Pools*. in International Conference of Vapor Cloud Modeling, Boston, Massachusetts, USA, AIChE, 1987.

16. Webber, D.M., *A Model for Pool Spreading and Vaporisation and its Implementation in the Computer Code GASP*, UKAEA SRD R507, 1990.

17. van Limpt, H., R. Beerkens, A. Lankhorst, and A. Habraken, *Mass transfer relations for transpiration evaporation experiments.* Int. J. Heat Mass Transfer, **48**, p5265-4281, 2005.

18. Incropera, F.P. and D.P. Dewitt, *Fundamentals of Heat and Mass Transfer*, New York, John Wiley & Sons, Inc., 1985.

19. Ambrosini, W., N. Forgione, A. Manfredini, and F. Oriolo, *On various forms of the heat and mass transfer analogy: Discussion and application to condensation experiments.* Nuclear Eng. Design, **236**, p1013-1027, 2006.

20. Craft, T.J., L.J.W. Graham, and B.E. Launder, *Impinging jet studies for turbulence model assessment - II. An examination of the performance of four turbulence models.* Int. J. Heat Mass Transfer, **36**(10), p2685-2697, 1993.

21. Heyerichs, K. and A. Pollard, *Heat transfer in separated and impinging turbulent flows.* Int. J. Heat Mass Transfer, **39**(12), p2385-2400, 1996.

22. Behnia, M., S. Parneix, and P. Durbin, *Numerical study of turbulent heat transfer in confined and unconfined impinging jets.* Int. J. Heat Mass Transfer, **41**(12), p1845-1855, 1998.

23. Chung, Y.M., K.H. Luo, and N.D. Sandham, *Numerical study of momentum and heat transfer in unsteady impinging jets.* Int. J. Heat Fluid Flow, **23**, p592-600, 2002.

24. Angioletti, M., R.M. Di Tommaso, E. Nino, and G. Ruocco, *Simultaneous visualization of flow field and evaluation of local heat transfer by transitional impinging jets.* Int. J. Heat Mass Transfer, **46**, p1703-1713, 2003.

Published by the Health and Safety Executive 07/12

HSE

Health and Safety Executive

Flammable vapour cloud risks from tank overfilling incidents

This report documents research undertaken in 2007 and 2008 to examine the important factors affecting the production of flammable vapour in incidents where large storage tanks of volatile liquids are overfilled. This is an important output from the Buncefield response programme that was not published on completion due to constraints on HSL staff involved in the investigation arising from the legal case. The work was summarised for the Process Safety Leadership report but has not been published in full.

It includes much useful information arising from a joint study of tank designs carried out with Shell Global Solutions. The analysis describes how different tank designs are likely to behave in an overflow situation, and the impact on the production rate of flammable vapour. It also contains the results of some early Computational Fluid Dynamics (CFD) modelling studies into the vapourisation of volatile components of multi component hydrocarbon mixtures. Simulations are presented that examine the effect of a number of factors on the vapour cloud behaviour, including the bund shape and location, tank proximity, presence of obstacles and spray pattern from the overfilling tank.

The work provides a first step towards developing a mathematical model to predict the size of flammable vapour clouds from overfilling releases, based on simple measures such as the tank dimensions, tank design type, pumping rates and liquid composition.

This work highlights the fact that there are important processes occurring at the bottom of the cascade near to the tank base that were not well understood at the time the report was completed, most notably splashing and pool evaporation. These issues have been explored in a later research report RR908.

This report and the work it describes were funded by the Health and Safety Executive (HSE). Its contents, including any opinions and/or conclusions expressed, are those of the authors alone and do not necessarily reflect HSE policy.

RR937

www.hse.gov.uk